CHEMISTRY
A EUROPEAN JOURNAL

DOI: 10.1002/chem.200801566

Pyrrolidinium Ionic Liquid Crystals

Karel Goossens, Kathleen Lava, Peter Nockemann, Kristof Van Hecke, Luc Van Meervelt, Kris Driesen, Christiane Görller-Walrand, Koen Binnemans, and Thomas Cardinaels*[a]

Abstract: *N*-Alkyl-*N*-methylpyrrolidinium cations have been used for the design of ionic liquid crystals, including a new type of uranium-containing metallomesogen. Pyrrolidinium salts with bromide, bis(trifluoromethylsulfonyl)-imide, tetrafluoroborate, hexafluorophosphate, thiocyanate, tetrakis(2-thenoyltrifluoroacetonato)europate(III) and tetrabromouranyl counteranions were prepared. For the bromide salts and tetrabromouranyl compounds, the chain length of the alkyl group C_nH_{2n+1} was varied from eight to twenty carbon atoms ($n=8$, 10–20). The compounds show rich mesomorphic behaviour: highly ordered smectic phases (the crystal smectic E phase and the uncommon crystal smectic T phase), smectic A phases, and hexagonal columnar phases were observed, depending on chain length and anion. This work gives better insight into the nature and formation of the crystal smectic T phase, and the molecular requirements for the appearance of this highly ordered phase. This uncommon tetragonal mesophase is thoroughly discussed on the basis of detailed powder X-ray diffraction experiments and in relation to the existing literature. Structural models are proposed for self-assembly of the molecules within the smectic layers. In addition, the photophysical properties of the compounds containing a metal complex anion were investigated. For the uranium-containing mesogens, luminescence can be induced by dissolving them in an ionic liquid matrix. The europium-containing compound shows intense red photoluminescence with high colour purity.

Keywords: ionic liquids · liquid crystals · metallomesogens · pyrrolidinium cations · uranium

Introduction

Ionic liquid crystals are a fascinating class of molecular materials, both from fundamental and from applied points of view.[1] The ionic nature of these compounds allows uncommon mesophases like the crystal smectic T phase[2–6] and the nematic columnar phase to be obtained.[7] Aligned samples of ionic liquid crystals show pronounced anisotropic ion conduction and are of interest as low-dimensional ion-conductive materials.[8,9] Recent studies have shown that ionic metallomesogens can be used as an anisotropic reaction medium for shape-selective synthesis of nanoparticles.[10–12] Different types of ionic liquid crystals have been investigated, among others imidazolium,[13–18] pyridinium,[13,16,19–22] quaternary ammonium[2–4,23] and quaternary phosphonium salts.[24,25] Recently, we reported on nematic ionic liquid crystals and a luminescent tetrakis β-diketonate lanthanidomesogen with mesogenic imidazolium cations.[26] The liquid-crystalline behaviour of the ionic salts strongly depends on the nature of both the cation and the anion, but also on the length of the alkyl chain of the organic cation. Pyrrolidinium salts are used as ionic liquids with a large electrochemical window,[27–29] as surfactants,[30] and as mesostructuring agents in the preparation of oriented thin films.[31] To the best of our knowledge, no investigation of the mesomorphic properties of thermotropic liquid-crystalline pyrrolidinium salts has appeared in the literature yet. However, the pyrrolidinium core offers advantages for studying the metal-centred luminescence of ionic metallomesogens, because it shows no inconvenient background fluorescence. Here we describe the

[a] K. Goossens, K. Lava, Dr. P. Nockemann, Dr. K. Van Hecke, Prof. Dr. L. Van Meervelt, Dr. K. Driesen, Prof. Dr. C. Görller-Walrand, Prof. Dr. K. Binnemans, Dr. T. Cardinaels
Katholieke Universiteit Leuven, Department of Chemistry
Celestijnenlaan 200F, PO Box 2404, 3001 Leuven (Belgium)
Fax: (+32) 16 327992
E-mail: thomas.cardinaels@chem.kuleuven.be

Supporting information for this article is available on the WWW under http://dx.doi.org/10.1002/chem.200801566. It contains synthetic procedures and characterisation data for $UO_2Br_2{\cdot}xH_2O$ and **13**; stack column graphs showing the evolution of the transition temperatures in the series **2a**–**12a** and **2g**–**12g**; powder X-ray diffraction data for uranyl complexes **6g**–**12g**; and powder X-ray diffractograms of **12a** and **12g** in the SmA phase.

thermotropic liquid-crystalline properties of *N*-alkyl-*N*-methylpyrrolidinium salts with bromide, bis(trifluoromethylsulfonyl)imide, tetrafluoroborate, hexafluorophosphate, thiocyanate, tetrakis(2-thenoyltrifluoroacetonato)europate(III) and tetrabromouranyl counteranions. In addition, the luminescence properties of the mesogens that contain a metal complex anion were studied.

Results and Discussion

Synthesis: Synthesis of the pyrrolidinium salts is outlined in Scheme 1. Compounds **1a**–**12a** were prepared by quaternisation (Menschutkin reaction) of 1-methylpyrrolidine with $C_nH_{2n+1}Br$ ($n=8$, 10–20).[32] Yields were in the range of 72–88% (except for **1a** and **2a**: 47 and 51%, respectively). Under the experimental conditions used, **1a** and **2a** were obtained as monohydrate salts, as confirmed by CHN elemental analysis, while **3a**–**12a** were obtained as water-free compounds and stored in a desiccator. Compounds **10b**–**10e** were synthesised by a metathesis reaction between bromide salt **10a** and lithium bis(trifluoromethylsulfonyl)imide ($LiNTf_2$, $Tf=SO_2CF_3$), sodium tetrafluoroborate, potassium hexafluorophosphate and potassium thiocyanate, respectively. Compound **10f** was prepared by a reaction between bromide salt **10a**, 2-thenoyltrifluoroacetone (Htta), sodium hydroxide and europium(III) chloride hexahydrate. Compounds **1g**–**12g** were synthesised by reaction of bromide salts **1a**–**12a** with uranyl bromide hydrate ($UO_2Br_2{\cdot}xH_2O$) in refluxing ethanol. Due to its hygroscopic character, it is difficult to determine the exact number of water molecules x in the uranyl bromide salt precursor. The uranyl bromide salt was carefully dried, and when weighing, x was assumed to be zero so that compounds **1g**–**12g** would not be contaminated with an excess of uranyl bromide. The uranyl complexes were obtained as anhydrous yellow solids (as confirmed by CHN elemental analysis), although no special care was taken to prevent hydration of the salts. The ^1H and ^{13}C NMR spectra of the uranyl complexes in CD_3OD (not reported here) are similar to those obtained for the parent halide salts in CD_3OD. The uranyl complexes were obtained in relatively low yields because of their rather good solubility in ethanol, from which they were recrystallised, and the difficulty of working with the hygroscopic uranyl bromide salt precursor (see above).

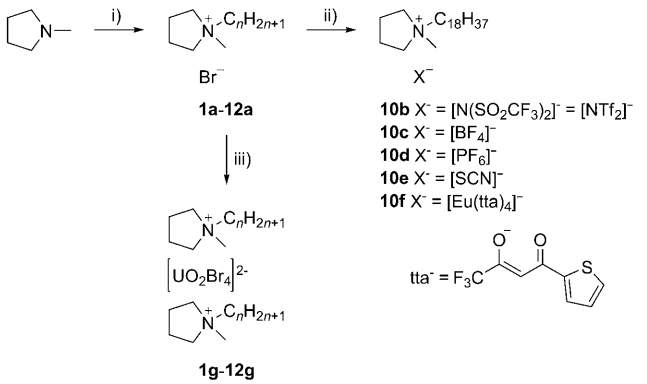

Scheme 1. Synthesis of the pyrrolidinium compounds. i) $C_nH_{2n+1}Br$ ($n=8$, 10–20), Ar, dry toluene, RT (**1a** and **2a**) or 80°C (**3a**–**12a**); ii) **10b**: **10a**, $LiNTf_2$, H_2O/MeOH, 60°C; ii) **10c**: **10a**, $NaBF_4$, acetone, reflux; ii) **10d**: **10a**, KPF_6, H_2O/MeOH, 60°C; ii) **10e**: **10a**, KSCN, Ar, acetone, 55°C; ii) **10f**: **10a**, Htta, NaOH, $EuCl_3{\cdot}6H_2O$, H_2O/EtOH, 50°C; iii) $UO_2Br_2{\cdot}xH_2O$, EtOH, reflux.

Single-crystal X-ray diffraction: Crystals of uranyl complex **6g** suitable for single-crystal X-ray structure determination could be obtained by slowly evaporating a solution of the compound in ethanol. The crystal structure consists of two crystallographically independent *N*-methyl-*N*-tetradecylpyrrolidinium cations and a $[UO_2Br_4]^{2-}$ ion in the asymmetric unit (Figure 1, top). In the first coordination sphere, the uranyl ion is surrounded by four bromide ions in the equatorial plane. Weak interactions of the protons of the pyrrolidinium cations with the bromine atoms (ranging from 2.75 to 3.04 Å) and with the oxygen atoms (ranging from 2.43 to 2.59 Å) of the $[UO_2Br_4]^{2-}$ ions are found (Figure 1, bottom). In the packing of the crystal structure of **6g**, the cationic head groups and the $[UO_2Br_4]^{2-}$ anions are arranged in

Abstract in Dutch: *Het* N-*alkyl*-N-*methylpyrrolidiniumkation werd gebruikt voor de bereiding van ionische vloeibare kristallen, waaronder een nieuw type uraniumhoudend metallomesogeen. Er werden pyrrolidiniumzouten met bromide-, bis(trifluoromethylsulfonyl)imide-, tetrafluoroboraat-, hexafluorofosfaat-, thiocyanaat-, tetrakis(2-thenoyl-trifluoroacetonato)europaat(III)- en tetrabromouranyl-anionen gesynthetiseerd. In het geval van de bromidezouten en de tetrabromouranylverbindingen werd de ketenlengte gevarieerd van acht tot twintig koolstofatomen (*n*=*8*, *10*, *11*, *12* ,*13*, *14*, *15*, *16*, *17*, *18*, *19*, *20). De verbindingen vertonen een rijk mesofasegedrag, van hooggeordende smectische fasen (de kristal-smectische E fase en de zeldzame kristal-smectische T fase) over smectische A fasen tot hexagonaal kolomvormige fasen, afhankelijk van de ketenlengte en het anion. Dit werk geeft een beter inzicht in de aard en vorming van de kristal-smectische T fase, en de moleculaire vereisten voor het voorkomen van deze hooggeordende fase. Er wordt een nauwkeurige beschrijving gegeven van de mesofasestructuur, op basis van gedetailleerde poeder X-stralendiffractie-experimenten en door het verband te leggen met de bestaande literatuur omtrent deze ongewone tetragonale mesofase. Er worden structurele modellen voorgesteld die de zelforganisatie van de moleculen in de smectische lagen verduidelijken. Daarnaast werden de fotofysische eigenschappen van de verbindingen met een anionisch metaalfragment onderzocht. Voor de uraniumhoudende metallomesogenen werd aangetoond dat luminescentie geïnduceerd kan worden door deze op te lossen in een ionische vloeistof. De europiumhoudende verbinding vertoont een intense rode fotoluminescentie met een hoge kleurzuiverheid.*

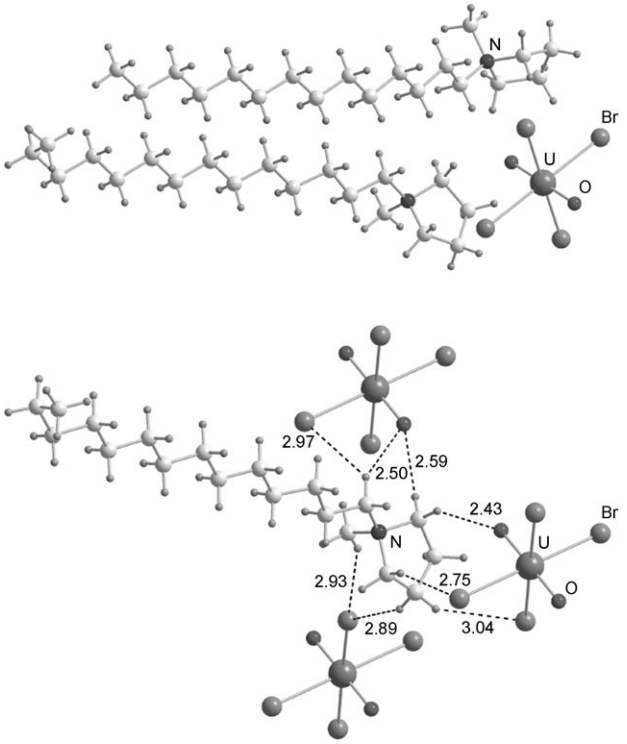

Figure 1. Top: asymmetric unit of the crystal structure of **6g**. Bottom: weak interactions of protons of the pyrrolidinium cations with the surrounding anions, shown for one of the cations in the crystal structure of **6g**.

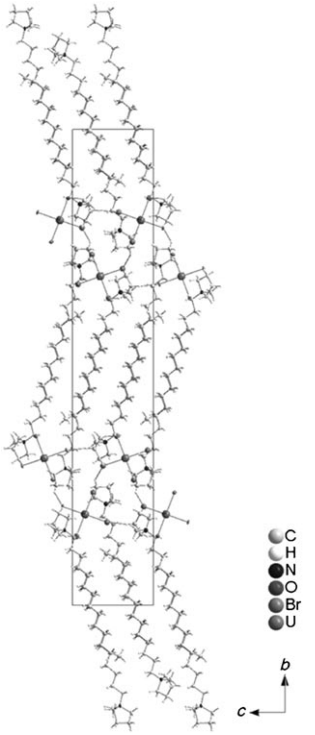

Figure 2. Packing in the crystal structure of **6g**, viewed along the *a* axis.

ionic double layers with the alkyl chains pointing in opposite directions (Figure 2). These double layers are separated from one another by the alkyl chains, which are arranged in a parallel and interdigitated fashion. The horizontal U···U distance within the double layers is 10.52 Å, and the vertical U···U distance is 8.57 Å. The shortest U···U distances between two parallel double layers are 22.14 and 35.64 Å between the inner and outer uranyl ions, respectively.

Thermal behaviour: The thermal properties of all compounds were examined by polarising optical microscopy (POM), differential scanning calorimetry (DSC) and X-ray diffraction on powder samples. The transition temperatures and thermal data for all the pyrrolidinium salts are collected in Table 1. Representative DSC traces of **6a**, **10a** and **10g** are shown in Figure 3. In general, the second heating run was not analogous to the first one, because the pyrrolidinium compounds are not stable at high temperatures (above ca. 200 °C). This was confirmed by POM, by the fact that the baseline of the DSC thermogram alters above approximately 200 °C, and by thermogravimetry (Figure 4). If the compounds were heated to only 180 °C during the first heating run, a matching and reproducible cooling run and a reproducible second heating run were obtained (Figure 5). According to thermogravimetry, the pyrrolidinium bromide compounds are thermally less stable than the corresponding uranyl complexes (Figure 4a). At 250 °C, **10a** showed 28 % weight loss, while **10g** had not started to decompose yet. The alkyl chain length does not seem to have any influence on the thermal stability of the pyrrolidinium bromides. On the other hand, the type of anion strongly determines the thermal stability (Figure 4b). Bis(trifluoromethylsulfonyl)-imide compound **10b** is thermally stable up to 365 °C. The thermal stability order of the singly charged anions can be summarised as: $NTf_2^- > PF_6^- > [Eu(tta)_4]^- > Br^- \approx BF_4^- > SCN^-$. Compound **10c** shows a two-stage decomposition process. The weight loss for compound **10f** occurring between 265 and 340 °C corresponds to the gradual decomposition of the metal-containing anion $[Eu(tta)_4]^-$.

For some compounds, two or more crystalline phases were observed. This is not unusual, as crystal polymorphism and the existence of conductive plastic crystal phases (rotationally disordered phases) of pyrrolidinium-based ionic liquids have been reported in the past.[27,29,33–35] A minimum alkyl chain length of eleven carbon atoms is required for the pyrrolidinium bromide salts to exhibit mesomorphism. Investigation of the thermal properties of **1a** and **2a** was complicated by their hygroscopicity and by the fact that different crystal forms melt at different temperatures in the case of samples without a thermal history. As a consequence, crystals of a high-melting polymorph are scattered in the melt of a lower-melting crystal polymorph when viewed by POM. The first and second DSC heating runs differed from one another when samples that had not been kept under an inert atmosphere were measured in DSC pans with a small hole in the lid. The transition temperatures for the third and fourth heating run were identical to the values observed for

Table 1. Transition temperatures and thermal data for the pyrrolidinium salts.

Compd	n[a]	Anion	Transition[b]	T [°C][c]	ΔH [kJ mol^{-1}] (ΔS [J K^{-1} mol^{-1}])	Compd	n[a]	Anion	Transition[b]	T [°C][c]	ΔH [kJ mol^{-1}] (ΔS [J K^{-1} mol^{-1}])
1a	8	Br^-	Cr→I	159	7.1 (16)	**1g**	8	$[UO_2Br_4]^{2-}$	Cr→I	67	11.7 (34)
2a	10	Br^-	Cr_1→Cr_2[d]	41	18.6 (59)	**2g**	10	$[UO_2Br_4]^{2-}$	Cr_1→Cr_2	57	4.0 (12)
			Cr_2→I	162	6.7 (15)				Cr_2→I	84	5.8 (16)
3a	11	Br^-	Cr→T_1	27	10.2 (34)	**4g**	12	$[UO_2Br_4]^{2-}$	Cr_1→Cr_2	61	11.6 (35)
			T_1→T_2	70	0.5 (1.4)				Cr_2→I	108	7.0 (18)
			T_2→I	171	5.7 (13)	**5g**	13	$[UO_2Br_4]^{2-}$	Cr_1→Cr_2	45	48.9 (154)
4a	12	Br^-	Cr→T_1[d]	53	32.7 (100)				Cr_2→I	109	5.4 (14)
			T_1→T_2	78	0.8 (2)	**6g**	14	$[UO_2Br_4]^{2-}$	Cr_1→Cr_2	49	50.0[e]
			T_2→I	191	6.7 (14)				Cr_2→E	55	
5a	13	Br^-	Cr_1→Cr_2	53	13.8[e]				(I→Col_h)	–[h]	–[h]
			Cr_2→T_1	59					E→I	133	6.4 (16)
			T_1→T_2	79	0.9 (3)	**7g**	15	$[UO_2Br_4]^{2-}$	Cr→E	60	74.2 (223)
			T_2→I	201	7.6 (16)				(I→Col_h)	–[h]	–[h]
6a	14	Br^-	Cr→T_1[d]	62	41.6 (124)				E→I	147	6.7 (16)
			T_1→T_2	80	0.9 (3)	**8g**	16	$[UO_2Br_4]^{2-}$	Cr→E	64	47.0 (139)
			T_2→I	208	8.7 (18)				(I→Col_h)	151[h]	–[h]
7a	15	Br^-	Cr→T_2	74	17.2 (50)				E→I	160	7.3 (17)
			(T_2→T_1)	83[f]	0.9 (3)[f]	**9g**	17	$[UO_2Br_4]^{2-}$	Cr_1→Cr_2	69	80.9[e]
			T_2→I	214	9.3 (19)				Cr_2→E	72	
8a	16	Br^-	Cr_1→Cr_2[d]	66	31.4[e]				(I→Col_h)	–[h]	–[h]
			Cr_2→T_2	75					E→I	169	7.6 (17)
			(T_2→T_1)	77[f]	0.8 (2)[f]	**10g**	18	$[UO_2Br_4]^{2-}$	Cr_1→Cr_2	62	11.2 (33)
			T_2→I	217	9.7 (20)				Cr_2→E	72	41.2 (118)
9a	17	Br^-	Cr_1→Cr_2	38[g]	1.1 (4)				E→I	172	10.0 (22)
			Cr_2→T	82	24.9 (70)	**11g**	19	$[UO_2Br_4]^{2-}$	Cr_1→Cr_2	75	96.8[e]
			T→I	218	9.3 (19)				Cr_2→E	80	
10a	18	Br^-	Cr_1→Cr_2	42	2.4 (8)				E→SmA	185	9.2 (20)
			Cr_2→T	82	26.4 (74)				SmA→I	227	0.5 (1.1)
			T→SmA	217	8.1 (17)	**12g**	20	$[UO_2Br_4]^{2-}$	Cr_1→Cr_2	41	2.8 (9)
			SmA→I	229	1.6 (3)				Cr_2→Cr_3	69	11.2 (33)
11a	19	Br^-	Cr_1→Cr_2	35[g]	1.1 (4)				Cr_3→E	83	50.2 (141)
			Cr_2→T	89	29.3 (81)				E→SmA	186	8.5 (19)
			T→SmA	216	8.3 (17)				SmA→I	267	0.8 (2)
			SmA→I	233	1.5 (3)						
12a	20	Br^-	Cr→T	89	32.7 (90)						
			T→SmA	214	8.9 (18)						
			SmA→I	233	1.3 (3)						
10b	18	NTf_2^-	Cr_1→Cr_2	34[g]	1.5 (5)						
			Cr_2→I	72	32.3 (94)						
10c	18	BF_4^-	Cr_1→Cr_2	47	7.8 (24)						
			Cr_2→T	92	20.8 (57)						
			T→I	166	5.5 (13)						
10d	18	PF_6^-	Cr→T	95	33.1 (90)						
			T→I	145	4.7 (11)						
10e	18	SCN^-	Cr_1→Cr_2	37	3.6 (12)						
			Cr_2→SmA	86	29.9 (83)						
			SmA→I	164	0.9 (2)						
10f	18	$[Eu(tta)_4]^-$	Cr→I	121	46.5 (118)						

[a] n = number of carbon atoms in the alkyl chain. [b] Abbreviations: Cr, Cr_1, Cr_2 and Cr_3 = crystalline or partially crystalline phase; T, T_1 and T_2 = crystal smectic T phase; E = crystal smectic E phase; SmA = smectic A phase; Col_h = hexagonal columnar phase; I = isotropic liquid. Transitions in parentheses indicate transitions to a monotropic mesophase. [c] Onset temperatures obtained by DSC at heating/cooling rates of 10 °C min^{-1} (He atmosphere). For **1a**–**12a**, **10c** and **10d**, values were taken from the second heating run (first heating run up to 180 °C). For the other compounds, values were taken from the first heating run. During the first cooling run, **1a**, **2a** and **1g**–**12g** were cooled to −50 °C, and the other compounds to −20 °C. [d] Before this endothermic transition, an exothermic recrystallisation process took place. For **2a**: at 9 °C (peak temperature) (ΔH = −15.2 kJ mol^{-1}; ΔS = −54 J K^{-1} mol^{-1}); for **4a**: at 23 °C (peak temperature) (ΔH = −9.7 kJ mol^{-1}; ΔS = −33 J K^{-1} mol^{-1}); for **6a**: at 33 °C (peak temperature) (ΔH = −18.5 kJ mol^{-1}; ΔS = −60 J K^{-1} mol^{-1}); for **8a**: at 53 °C (peak temperature) (ΔH = −5.6 kJ mol^{-1}; ΔS = −17 J K^{-1} mol^{-1}). [e] As the transition peaks in the DSC thermogram were not fully resolved, the total enthalpy value ΔH for both transitions is given. [f] Values taken from the first cooling run (first heating run up to 180 °C). [g] Peak temperature. [h] Not detected by DSC. If possible, the temperature at which the monotropic mesophase transformed into the isotropic liquid phase on heating was determined by POM.

the second heating run. When the compounds were dried in vacuo at 180 °C (i.e., in their liquid state) for three hours and put in completely sealed DSC pans in a glove box, the first and second DSC heating run were almost identical to one another (slightly lower melting point for the second heating run) and the same peaks as for the second heating

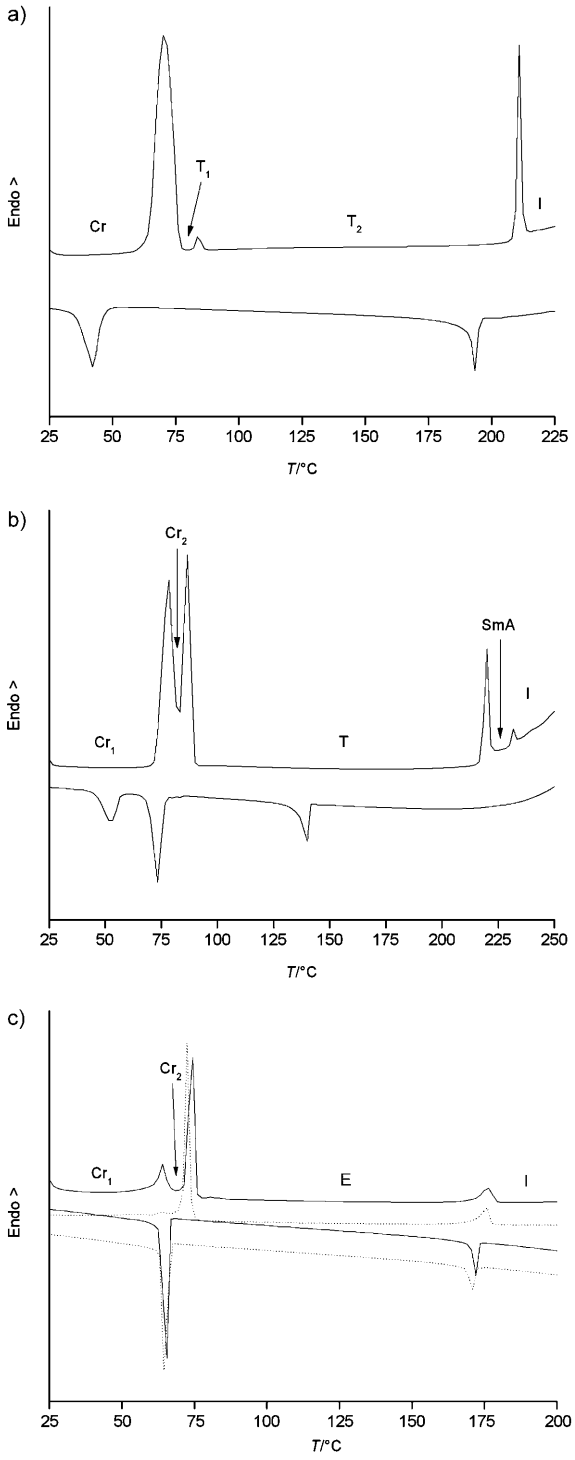

Figure 3. DSC traces of a) **6a**, b) **10a** and c) **10g** (heating/cooling rate of 10 °C min^{-1}; He atmosphere). The first heating/cooling cycle is shown by a solid line, and the second heating/cooling cycle by a dashed line. Abbreviations: Cr, Cr_1 and Cr_2 = crystalline or partially crystalline phase; T, T_1 and T_2 = crystal smectic T phase; E = crystal smectic E phase; SmA = smectic A phase; I = isotropic liquid. Endothermic peaks point upwards.

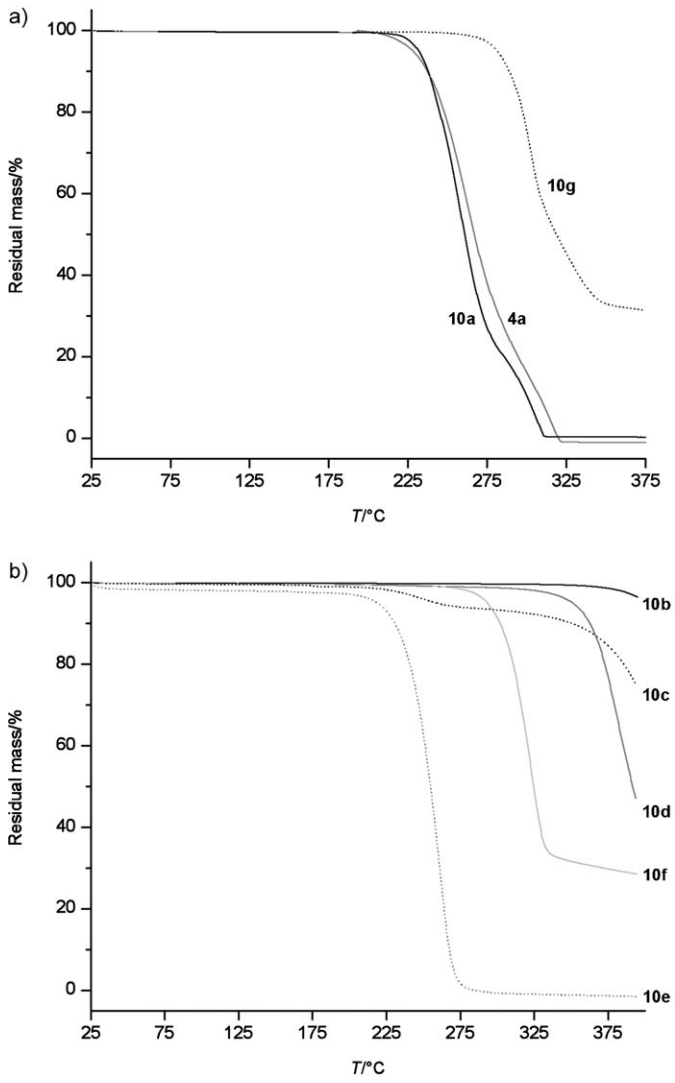

Figure 4. Thermograms of selected pyrrolidinium salts (heating rate of 10 °C min^{-1}; N_2 atmosphere). a) **4a**, **10a** and **10g**; b) **10b**, **10c**, **10d**, **10e** and **10f**.

run of the first series of measurements were observed. The melting temperatures were, however, lower (by 3–5 °C) after the drying procedure. This might be due to slight decomposition, as indicated by the change in colour from white to pale brown.

Bromide salts **3a**–**12a** showed one or more enantiotropic smectic phases. Compounds **3a**, **4a**, **5a** and **6a** (n = 11, 12, 13 and 14, respectively) formed two types of crystal smectic T phases (for a discussion on the T phase, see the section about X-ray diffraction experiments), designated as T_1 and T_2 for the lower- and higher-temperature phase, respectively. The T_1 and T_2 phases appeared both on heating and on cooling (Figure 5a). Compounds **7a** and **8a** (n = 15 and 16, respectively) showed only one type of enantiotropic T phase (designated as T_2). However, on cooling, another T phase (designated as T_1) appeared beneath the enantiotropic T phase, as indicated by the appearance of an additional, small peak in the DSC thermograms. Compound **9a** (n = 17) exhibited only one type of T phase. Compounds **10a**, **11a** and **12a** (n = 18, 19 and 20, respectively) showed a SmA phase at higher temperatures and a T phase at lower tem-

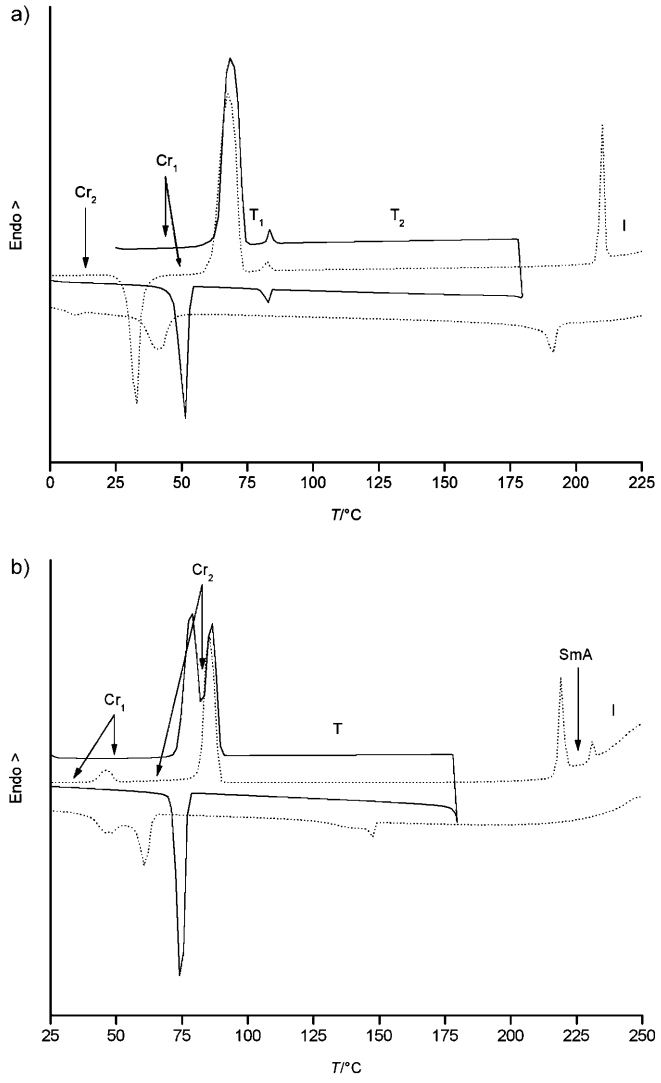

Figure 5. DSC traces of a) **6a** and b) **10a** (heating/cooling rate of 10 °C min^{-1}; He atmosphere). The first heating/cooling cycle is shown by a solid line, and the second heating/cooling cycle by a dashed line. Abbreviations: Cr_1 and Cr_2 = crystalline or partially crystalline phase; T, T_1 and T_2 = crystal smectic T phase; SmA = smectic A phase; I = isotropic liquid. Endothermic peaks point upwards.

peratures. The bis(trifluoromethylsulfonyl)imide salt **10b** was not liquid-crystalline. The tetrafluoroborate salt **10c** and the hexafluorophosphate salt **10d** showed a T phase, while the thiocyanate salt **10e** showed a SmA phase. Of the compounds containing metal complex anions, the tetrakis(2-thenoyltrifluoroacetonato)europate(III) salt **10f** was not liquid-crystalline, while the tetrabromouranyl salts with a chain length of at least fourteen carbon atoms (**6g–12g**) showed crystal smectic E phases. For compounds **6g–9g** (n = 14–17), an additional monotropic hexagonal columnar phase (Col_h) was observed on cooling from the isotropic liquid. Compounds **11g** and **12g** (n = 19 and 20, respectively) showed an additional SmA phase above the highly ordered smectic phase. Only a very limited number of uranium-containing liquid crystals have been reported till now.[36–40]

The SmA phases could be easily identified by their defect textures: focal conic fan and oily streak textures were observed (Figure 6, top right and middle left). For both the SmA and T phases, observation of large homeotropic domains confirmed that they are orthogonal, optically uniaxial mesophases. For the more viscous T phases, the observed lancet-like texture (Figure 6, top left) or mosaic texture points at a highly ordered smectic phase. On the basis of POM observations alone, these phases could not be unequivocally assigned as T phases (e.g., SmB and crystal B phases also show a lancet-like texture). X-ray diffraction measurements on powder samples were required for full characterisation of these phases (see below). A completely non-birefringent texture such as reported by Nogami et al.[41] and Ohta et al.[5] for the T phases of 1,4-dialkyl-1,4-diazoniabicyclo[2.2.2]octane dibromides was not observed for the T phases of the pyrrolidinium compounds described here (except for compound **10c**). Tetrabromouranyl salts **6g–12g** showed viscous mesophases for which lancet-like and mosaic textures, as well as large pseudo-homeotropic domains, were observed (Figure 6, middle right and bottom left). For the monotropic Col_h phase of **6g-9g**, a pseudo focal conic texture was seen (Figure 6, bottom right). In the case of **6g** and **9g**, the Col_h phase was observed upon cooling over a narrow temperature range for a very short period of time, while it was more stable in the case of **7g** and **8g**.

A contact sample of compound **8a** and *N*,*N*-bis(hexadecyl)-*N*,*N*-dimethylammonium bromide (**13**) was prepared by allowing a small droplet of **8a** in its T phase and a small droplet of **13** in its isotropic liquid state to mix under a cover slip at 180 °C. Compound **13** was one of the first compounds that was reported to exhibit a T phase (see below).[2] In the first heating run, it shows a crystal-to-crystal transition at 64 °C (ΔH = 5.6 kJ mol^{-1}; ΔS = 17 J K^{-1} mol^{-1}); its melting point and clearing point are 76 and 171 °C, respectively (ΔH_m = 54.8 kJ mol^{-1}; ΔS_m = 157 J K^{-1} mol^{-1}; ΔH_c = 7.6 kJ mol^{-1}; ΔS_c = 17 J K^{-1} mol^{-1}).[42] The interface between the two materials was studied by POM on cooling the contact sample from the isotropic liquid. Interestingly, the two compounds mixed homogeneously, and at the interface a SmA phase was formed (Figure 7). Apparently, the two different mesogens, both showing a T phase in their pure form, cannot form this highly ordered phase when they are mixed; a disordered SmA phase is formed instead. The difference in molecular structure (one chain per cation for **8a**; two chains per cation for **13**) and the difference in molecular packing in the T phases shown by both mesogens (ionic double layers for **8a** (see below); ionic monolayers for **13**[2]) preclude ordering of a mixture of the compounds in a square two-dimensional lattice.

In the series **3a–12a** and **6g–12g**, the melting and clearing temperatures increase on going from shorter to longer chain lengths. Such behaviour was also observed for mesomorphic imidazolium and pyridinium salts.[13,14,16,17,19,22] However, compared to the imidazolium and pyridinium salts, which only exhibit SmA phases, our pyrrolidinium salts show a rich polymorphism, ranging from several types of smectic

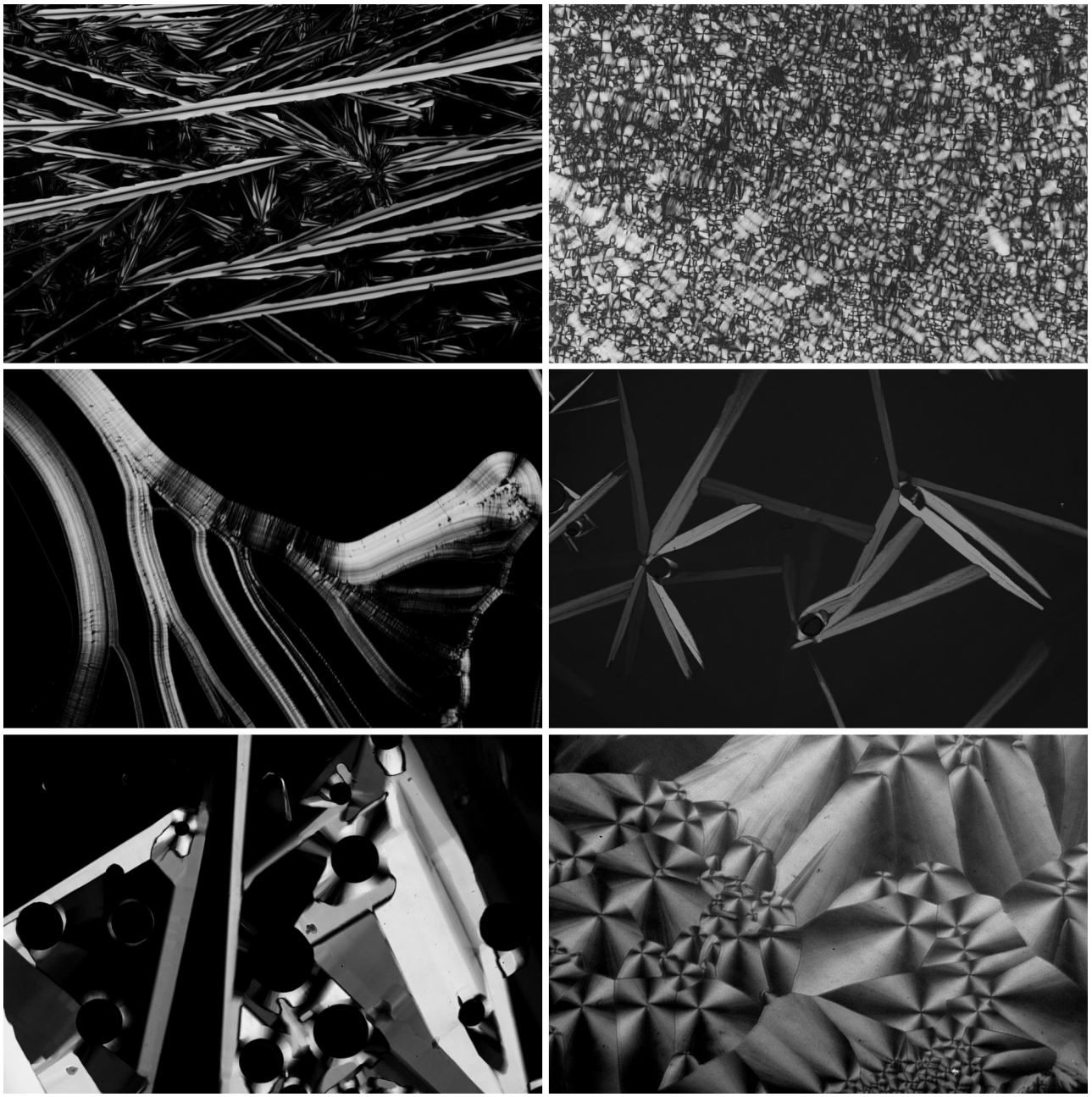

Figure 6. Top left: lancet-like texture of the T_2 phase of **6a** at 165 °C (100× magnification). Top right: focal conic fan texture of the SmA phase of **12a** at 215 °C (200× magnification). Middle left: oily streak texture of the SmA phase of **10e** at 130 °C (200× magnification). Middle right: lancet-like texture of the E phase of **6g** at 115 °C (100× magnification). Bottom left: mosaic texture of the E phase of **6g** at 99 °C (200× magnification). Bottom right: pseudo focal conic texture of the Col_h phase of **8g** at 150 °C (100× magnification).

phases to even a (monotropic) Col_h phase for some uranyl complexes. The difference can be attributed to the different shapes of the cationic head groups, the absence of charge delocalisation for pyrrolidinium cations and the absence of strong hydrogen bonding for *N*-alkyl-*N*-methylpyrrolidinium halides. Although short contacts exist in the crystalline solid state of *N*-methyl-*N*-propylpyrrolidinium iodide (between the halide anions and the β-protons of the pyrrolidinium cations), these interactions cannot be assigned as true hydrogen bonds because of the large distance between them.[43] On the other hand, the presence of non-classical C–H···X hydrogen bonding in halide salts with heteroaromatic cations has been described by several authors in the past.[44–47] The fact that a minimum alkyl chain length is required to induce mesomorphism has been commonly observed for ionic liquid crystals.[1] In the series **1a**–**12a**, an alkyl chain length of at least eleven carbon atoms is needed to obtain microphase separation between the ionic head groups and the hydrophobic alkyl chains, which leads to the formation of (highly ordered and disordered) lamellar phases. The micro-

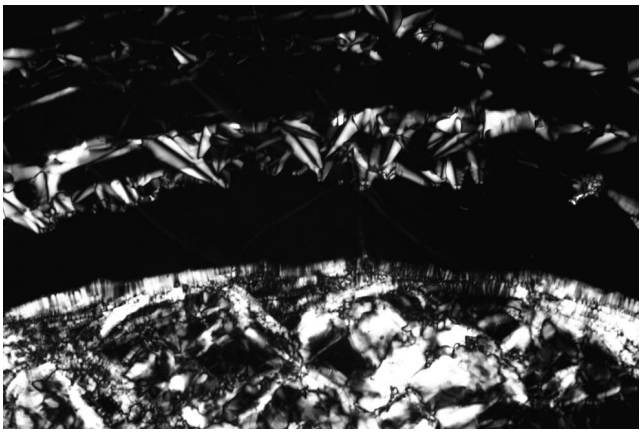

Figure 7. Contact preparation of **8a** and **13** at 163 °C (200× magnification) after cooling from 180 °C. Lower part: **8a** in its T phase. Upper part: **13** in its T phase. Middle part (interface between the two T phases): SmA phase (mostly homeotropically aligned; a focal conic fan texture appears when the sample is compressed with a needle).

phase separation is a result of the strong van der Waals interactions between the long aliphatic alkyl chains.

For compounds **10a**, **11a** and **12a**, a SmA phase is formed above the T phase. Such a phase sequence was also observed for *N*,*N*-bis(2-hydroxyethyl)-*N*-methyl-*N*-alkylammonium bromides.[4] However, for the latter compounds, the SmA phase was observed for a whole series of compounds ($n=12$, 14, 16 and 18 carbon atoms), whereas for our pyrrolidinium compounds, the SmA phase is only seen for the long-chain alkyl analogues ($n=18$, 19 or 20 carbon atoms). The T–SmA transition is a first-order transition which is accompanied by a considerable enthalpy change (8–9 kJ mol^{-1}). It appears that (very) long alkyl chains are not compatible with an ordered packing of the ions in the ionic sublayers at higher temperatures, and hence a disordered SmA phase results (see below).

For the series **6g–9g**, the appearance of columnar (besides smectic) mesomorphism was surprising. However, a Col_h phase was also observed for several *N*-alkylpyridinium salts with $[CuCl_4]^{2-}$ as counteranion ($n=12$, 13 or 14 carbon atoms).[22] The octahedral $[UO_2Br_4]^{2-}$ dianion has a different coordination geometry compared to the tetrahedral $[CuCl_4]^{2-}$ dianion and consequently has a different shape and size. The importance of the coordination geometry is illustrated by the fact that *N*-alkylpyridinium salts of the square-planar $[PdCl_4]^{2-}$ dianion only show smectic mesophases, while the corresponding $[CuCl_4]^{2-}$ salts exhibit columnar, cubic and smectic A mesophases.[22,48] It was also found that salts of the $[CoCl_4]^{2-}$, $[NiCl_4]^{2-}$, $[CuCl_4]^{2-}$, $[ZnCl_4]^{2-}$ and $[CdCl_4]^{2-}$ complex anions (tetrahedral coordination geometry) with *N*-hexadecylpyridinium cations have similar transition temperatures and mesophase temperature ranges, which on the other hand differ from those of the corresponding $[PdCl_4]^{2-}$ salt.[13,49] Although the pyrrolidinium compounds with two long alkyl chains per cation have not been synthesised yet, it can be expected that the corresponding uranyl complexes would be mesomorphic for shorter chain lengths than fourteen carbon atoms. It was observed that in the homologous series of $[C_n\text{mim}]_2[PdCl_4]$ complexes ($[C_n\text{mim}]^+$ = 1-methyl-3-alkylimidazolium) a minimum of 14 carbon atoms ($n=14$) is required to show liquid-crystalline properties, while $[C_8C_8\text{im}]_2[PdCl_4]$ already shows a SmA phase over a broad temperature range.[50,51]

In the series **10a–10g**, the anion clearly has great influence on the thermal behaviour.[14,52] The large NTf_2^- and $[Eu(tta)_4]^-$ anions (compounds **10b** and **10f**, respectively) destroy the liquid-crystalline properties, while for the smaller anions, the anion type has a large effect on the mesomorphic behaviour (mesophase type and transition temperatures). Compound **10a** exhibits both T and SmA phases, while compounds **10c** and **10d** only exhibit a T phase. Furthermore, when the bromide anion is replaced by a thiocyanate anion, as in compound **10e**, the highly ordered T phase is replaced by a disordered SmA phase. Apparently, the larger, non-spherical thiocyanate anion is not suitable for assembly in an ordered, square, two-dimensional network (see below). Combination of the *N*-methyl-*N*-octadecylpyrrolidinium cation with a $[UO_2Br_4]^{2-}$ dianion, as in **10g**, leads to formation of a crystal smectic E phase.

Powder X-ray diffraction: Most of the liquid-crystalline pyrrolidinium compounds were studied by X-ray diffraction on powder samples for further identification of the enantiotropic mesophases and to obtain more information about the molecular packing in the mesophases. Table 2 gives an overview of the Bragg reflections collected from the X-ray diffractograms of compounds **4a**, **6a**, **8a**, **10a**, **12a**, **10c**, **10d** and **10e**. Diffraction data for the uranyl complexes **6g-12g** are given in the Supporting Information.

Before describing and discussing the X-ray diffractograms of the mesophases formed by our pyrrolidinium compounds, we briefly discuss the nature of the T phase. The T phase is a highly ordered mesophase which has not often been observed and which has an unusual symmetry. The T phase was first observed in 1993 by Skoulios and co-workers, when they examined the thermal behaviour of *N*,*N*-dialkyl-*N*,*N*-dimethylammonium bromides.[2] On the basis of powder X-ray diffraction measurements, they concluded that, within the smectic layers, the lateral packing of the cationic head groups and bromide anions was ordered and tetragonal in symmetry. Therefore, the mesophase was named smectic T (according to Przedmojski and Dynarowicz-Łątka, this phase was only shown by the homologues with two hexadecyl or two octadecyl chains; the compounds with two decyl, two dodecyl or two tetradecyl chains were said to exhibit crystal smectic E phases[53]). More specifically, the ammonium and bromide ions were arranged periodically in a square two-dimensional network, and the ionic sublayers were separated from one another by sublayers containing the disordered alkyl chains. The T phases are rare, and until now they have only been observed for ionic liquid crystals: oxynitrostilbene derivatives of *N*,*N*-dialkyl-*N*,*N*-dimethylammonium bromides,[3] *N*,*N*-bis(2-hydroxyethyl)-*N*-methyl-*N*-alkylammonium bromides,[4] 1,4-dialkyl-1,4-diazoniabicyclo-

Table 2. Bragg reflections collected from the X-ray diffractograms of the different enantiotropic mesophases.

Compd	d_{meas} [Å][a]	I[b]	hkl[c]	d_{calcd} [Å][a]	Parameters of smectic phase[d–g]	Compd	d_{meas} [Å][a]	I[b]	hkl[c]	d_{calcd} [Å][a]	Parameters of smectic phase[d–g]
4a	27.80	VS	001	27.75	T_1: $T=70$ °C	**12a**	38.99	VS	001	38.92	T: $T=150$ °C
	–[h]		002		$V_M=574$ Å^3		19.50	M	002	19.46	$V_M=811$ Å^3
	9.25	M	003	9.25	$A_M=41.4$ Å^2		–[h]		003		$A_M=41.6$ Å^2
	6.93	M	004	6.94	$L=19.13$ Å		9.72	M	004	9.73	$a=6.38$ Å
	5.55	M	005	5.55			7.77	M	005	7.78	$L=29.32$ Å
	4.62	W	006	4.63			6.48	M	006	6.49	
	–[i]		110				5.56	M	007	5.56	
	–[i]		111				4.87	W	008	4.87	
	–[i]		200				4.51	M	110	4.51	
	–[i]		210				3.20	W	200	3.19	
	27.29	VS	001	27.28	T_2: $T=130$ °C		2.85	W (br)	210	2.85	
	–[h]		002		$V_M=599$ Å^3		35.74	VS	001	35.85	SmA: $T=200$ °C[j]
	9.08	M	003	9.09	$A_M=44.0$ Å^2		17.98	W	002	17.92	$V_M=839$ Å^3
	6.82	M	004	6.82	$a=6.39$ Å						$A_M=46.8$ Å^2
	5.46	M	005	5.46	$L=19.13$ Å						$L=29.32$ Å
	4.55	W	006	4.55		**10c**	32.63	VS	001	32.67	T: $T=130$ °C
	4.52	W	110	4.52			16.32	M	002	16.34	$V_M=762$ Å^3
	4.46	W	111	4.46			10.88	W	003	10.89	$A_M=46.6$ Å^2
	–[i]		200				8.17	M	004	8.17	$a=6.90$ Å
	–[i]		210				6.54	M	005	6.53	$L=26.73$ Å
6a	30.02	VS	001	30.06	T_1: $T=75$ °C		5.46	W	006	5.45	
	15.01	W	002	15.03	$V_M=625$ Å^3		4.88	M	110	4.88	
	10.01	M	003	10.02	$A_M=41.6$ Å^2		4.84	M	111	4.82	
	7.52	M	004	7.52	$a=6.28$ Å		4.68	W	112	4.67	
	6.02	M	005	6.01	$L=21.67$ Å		4.47	W	113	4.45	
	5.02	W	006	5.01			4.20	W	114	4.19	
	4.44	W	110	4.44			3.94	W	115	3.91	
	4.40	W	111	4.39			3.62	W	116	3.63	
	3.13	W	200	3.14			3.45	W	200	3.45	
	2.77	W	210	2.81			–[i]		210		
	30.02	VS	001	30.11	T_2: $T=130$ °C	**10d**	30.64	VS	001	30.71	T: $T=130$ °C
	15.09	W	002	15.05	$V_M=649$ Å^3		15.40	M	002	15.36	$V_M=866$ Å^3
	10.05	W	003	10.04	$A_M=43.2$ Å^2		10.25	M	003	10.24	$A_M=56.4$ Å^2
	7.52	M	004	7.53	$a=6.37$ Å		7.67	M	004	7.68	$a=7.29$ Å
	6.03	M	005	6.02	$L=21.67$ Å		6.14	M	005	6.14	$L=26.73$ Å
	5.01	W	006	5.02			5.16	W	110	5.16	
	4.50	W	110	4.50			5.12	W	006	5.12	
	4.47	W	111	4.45			–[k]		111		
	3.18	W	200	3.18			4.87	W	112	4.89	
	2.71	W	210	2.85			4.60	W	113	4.60	
8a	33.36	VS	001	33.13	T_2: $T=130$ °C		4.27	W	114	4.28	
	16.50	M	002	16.56	$V_M=700$ Å^3		3.94	W	115	3.94	
	11.00	W	003	11.04	$A_M=42.2$ Å^2		3.63	W (br)	200	3.65	
	8.28	M	004	8.28	$a=6.38$ Å		–[i]		210		
	6.63	M	005	6.63	$L=24.23$ Å	**10e**	34.12	VS	001	34.12	SmA: $T=125$ °C
	5.53	W	006	5.52							$V_M=708$ Å^3
	4.51	M	110	4.51							$A_M=41.6$ Å^2
	4.49	M	111	4.47							$L=26.73$ Å
	3.19	W	200	3.19							
	2.82	W (br)	210	2.85							
10a	35.96	VS	001	35.92	T: $T=150$ °C						
	17.98	M	002	17.96	$V_M=760$ Å^3						
	–[h]		003		$A_M=42.4$ Å^2						
	9.00	M	004	8.98	$a=6.37$ Å						
	7.18	M	005	7.18	$L=26.73$ Å						
	5.98	M	006	5.99							
	5.13	W	007	5.13							
	4.48	W	008	4.49							
	4.51	M	110	4.51							

Table 2. (Continued)

Compd	d_{meas} [Å][a]	I[b]	hkl[c]	d_{calcd} [Å][a]	Parameters of smectic phase[d–g]	Compd	d_{meas} [Å][a]	I[b]	hkl[c]	d_{calcd} [Å][a]	Parameters of smectic phase[d–g]
	3.20	W	200	3.19							
	2.84	W (br)	210	2.85							
	33.36	VS	001	33.45	SmA: $T=195\,^{\circ}C$[j]						
	16.77	W	002	16.73	$V_M=784$ Å^3						
					$A_M=46.8$ Å^2						
					$L=26.73$ Å						

[a] d_{meas} and d_{calcd} are the measured and calculated diffraction spacings, respectively. [b] I is the intensity of the reflections: VS, very strong; M, medium; W, weak; br, broad reflection. [c] hkl are the Miller indices of the reflections. [d] T is the temperature at which the X-ray diffractogram was recorded. [e] V_M is the molecular volume, and A_M the molecular area. [f] a is the lattice parameter of (the square basis of) the tetragonal unit cell in the T phase ($a=b$, $c=d$). For compound **4a**, a could not be determined due to the absence of signals in the wide-angle region. [g] L is the calculated length of the relevant pyrrolidinium cation in its most extended conformation (estimated with Chem3D; the structure of the pyrrolidinium cation was energy-minimised by an MM2 calculation within Chem3D). [h] Not detected because of overlap with the diffraction signal produced by the covering foil used in the experimental set-up (this signal occurs at $2\theta=5.7$–$7.6°$). [i] Not detected. [j] During the temperature scan of the X-ray diffraction measurement, the SmA phase was observed at lower temperatures than indicated by DSC (Table 1). This might point to slight decomposition of the sample at high temperatures. [k] This reflection overlaps with the (006) reflection.

[2.2.2]octane dibromides[5] and 1,4-piperazinium dialkyl sulfates.[6] For the highly ordered smectic (and crystal smectic) phases formed by non-ionic calamitic mesogens, only hexagonal (hexatic phases) and rectangular two-dimensional networks have been observed so far, in which the molecules can be tilted or non-tilted within the smectic layers.[54,55] Considering the type and structure of the cation, T phases have only been observed for salts with cations carrying one or two non-delocalised charges, similar to the pyrrolidinium compounds described in this paper (on the contrary, unfunctionalised 1-methyl-3-alkylimidazolium and *N*-alkylpyridinium bromides invariably form disordered SmA phases). For these compounds, localised coulombic interactions result in an ordered packing of the ions in the ionic sublayers; no other relevant interactions must be taken into account (the cations do not carry any functional groups). Ordering of the ions in a square two-dimensional network with cations and anions in the corners and centres, respectively, allows strict alternation of positive and negative charges (in a manner similar to that found in the faces of the face-centred cubic crystals of alkali metal halides). In this way, positive and negative charges compensate each other most efficiently.

The following section describes the X-ray diffraction data of our pyrrolidinium compounds. The crystalline nature of the solid phases at room temperature was confirmed by the presence of several sharp Bragg reflections at both small and wide angles. In addition, the equidistant small-angle reflections indicated that the molecules are arranged in a lamellar fashion.

The diffractograms of the smectic mesophases show several sharp and equidistant reflections at small angles in the case of the highly ordered smectic phases (crystal smectic T and crystal smectic E), or only two sharp and equidistant reflections at small angles in the case of the SmA phases (except for **10e**, for which only one sharp reflection was observed). These reflections are related to the consecutive smectic layers of a specific layer thickness d (Table 2). The absence of more small-angle reflections for the SmA phases confirms that the positions of the strongly diffracting bromide anions in the SmA layers are not as well-defined as in the crystal smectic T layers. In the wide-angle region, a diffuse signal, centred at about 4.7 Å, was observed, corresponding to the lateral short-range order of the disordered (molten) aliphatic chains. In addition, several relatively sharp peaks were seen in the wide-angle region for the T and E phases. For the E phases, additional peaks were observed in the medium-angle region (see Supporting Information). The nature of the T phase of **4a** could not be unequivocally confirmed by X-ray diffraction due to the absence of signals in the wide-angle region. Nevertheless, we believe that this assignment is justified because **4a** shows identical defect textures and similar enthalpy values compared to **6a**. In addition, Skoulios et al. also observed less and less intense wide-angle reflections for the shortest chain compound in comparison to the other ammonium bromides.[4]

The T phases shown by the pyrrolidinium bromide compounds were identified by the presence of two rather sharp peaks (located at about 4.5 and 3.2 Å) and one low-intensity peak (located around 2.8 Å) in the wide-angle region (Figure 8). These peaks were indexed as the (110), (200) and (210) reflections of a square lattice [reciprocal spacings of the reflections in the characteristic ratio $1:2^{1/2}:(5^{1/2}/2^{1/2})$].[2] The low-intensity (210) reflection broadens with increasing chain length. For compounds **4a**, **6a** and **8a**, the diffractograms additionally show the (111) reflection of a tetragonal lattice. This indicates that the smectic layers are slightly three-dimensionally correlated. Due to the shorter chains, the ionic sublayers are separated by a smaller distance (see below).[5,6]

In contrast to what is commonly observed for SmA phases, the layer thickness d of the T phase is independent of temperature (Figure 9). However, d increases linearly with the number of carbon atoms n in the alkyl chain [Eq. (1), Figure 10].

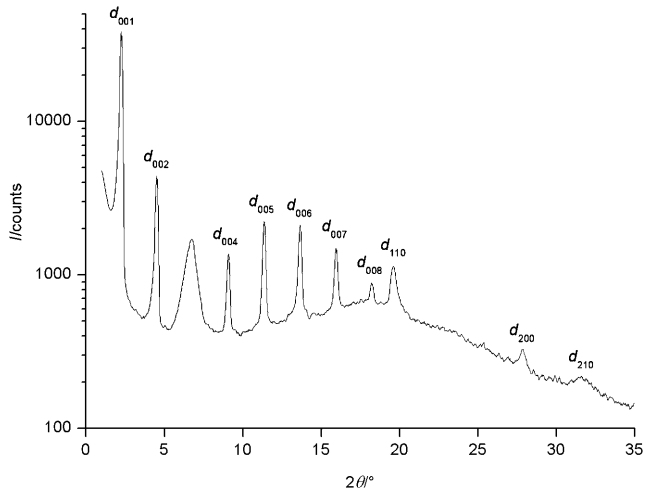

Figure 8. X-ray diffractogram of **12a** in the T phase at 150 °C, represented as the logarithm of the scattering intensity (in counts) versus the scattering angle 2θ (the broad diffraction signal centred at $2\theta \approx 6.5°$ is due to the covering foil used in the experimental set-up).

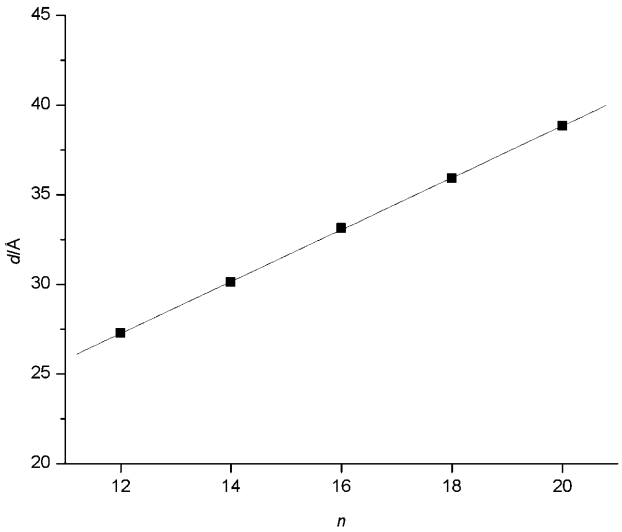

Figure 10. Evolution of the layer thickness d of the T phase at 130 °C as a function of the number of carbon atoms n in the alkyl chain for the series **3a**–**12a**: $d = 9.9(\pm 0.1) + 1.448(\pm 0.008)n$.

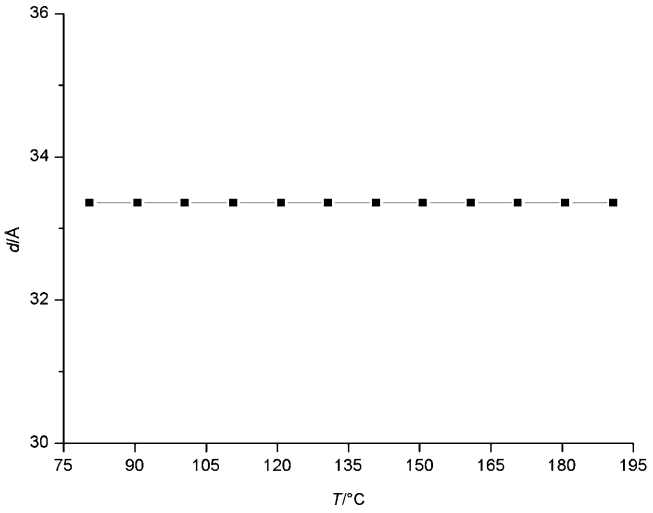

Figure 9. Evolution of the layer thickness d of the T phase of **8a** as a function of temperature.

$$d/\text{Å} = 9.9(\pm 0.1) + 1.448(\pm 0.008)n \quad (1)$$

As a consequence, the thickness of the ionic sublayers d_0 can be estimated to be approximately 9.9 Å. The unit cell parameter a of the square lattice (for a two-dimensional square lattice, $1/d_{hk}^2 = (h^2+k^2)/a^2$) only slightly increases with temperature (e.g., for compound **8a**: $a = 6.31$ Å at 90 °C, $a = 6.45$ Å at 170 °C). However, at a given temperature it is nearly constant for all chain lengths, and is on average equal to 6.37 Å at 130 °C. As noted by Skoulios et al., this lattice can only describe the periodic arrangement of the cationic head groups and the bromide anions in three-dimensional space, since the alkyl chains are disordered.[2,4] From a formal point of view, the T phase is a genuine crystal phase exhibiting three-dimensional positional order. On the other hand, Skoulios et al. explain in their paper why they prefer to consider the T phase, from a morphological point of view, as a truly smectic liquid-crystalline phase (with abbreviation SmT).[4] They state that the three-dimensional correlations in the T phase arise from long-range coulombic interactions of the ionic charges, which are periodically distributed inside the ionic sublayers according to a tetragonal lattice. However, as the coulombic interactions are stronger inside the polar layers than between them (especially when longer alkyl chains separate the ionic layers, which explains the fact that no (111) reflection was observed for **10a** and **12a** in their T phases), the smectic layers can slide over each other rather easily. We indeed observed that the T phases, although appreciably viscous, are soft and flowing. We propose to consider the T phase as a crystal smectic phase, and denote it by a capital letter T without the prefix "Sm". This type of abbreviation is also used for the other known crystal smectic (or anisotropic plastic crystal) phases, namely, the B, J, G, E, K and H phases.[54,55]

Interestingly, the unit-cell parameter a of the higher-temperature T_2 phase of compound **6a** differs only slightly from that of the lower-temperature T_1 phase (unfortunately, a could not be calculated for the T_1 phase of compound **4a**). This indicates that there are only subtle structural differences between the two T phases. This is supported by the very small enthalpy change that accompanies the T_1–T_2 phase transition of **4a** and **6a** (Table 1). Whereas the lamellar period of compound **4a** decreases on going from T_1 to T_2, it remains constant for **6a**. It is not justified to make any statements about the thickness of the ionic sublayers of the T_1 phases, as only two lamellar periods are available to plot as a function of the chain length n.

To provide a more precise description of the molecular arrangement, a quantitative discussion based on the measured periodicities and calculated (partial) molecular volumes is

presented. As the layer thickness $d = V/a^2 = (ZV_0 + ZV_{CH_2}n)/a^2$ (where V is the volume of the tetragonal unit cell, Z the number of molecules per unit cell, V_0 the volume of one ionic head group and V_{CH_2} the volume of one methylene unit; at 130 °C $V_{CH_2} \approx 29.2$ Å^3;[56] the volume contribution of the terminal methyl group is somewhat larger than that of a methylene group, but this is not taken into account), Z can be deduced from the slope of the linear d versus n plot (Figure 10). This calculation leads to a value of $Z \approx 2.0$. Therefore, each tetragonal unit cell contains two molecules, and consequently the ionic sublayer consists of two cationic head groups and two bromide anions per unit cell. The molecular volume V_M can be estimated by using the relation $V_M = (M/0.6022)f$, where M is the molecular mass (g mol^{-1}) and f is a temperature-correcting factor ($f = 0.9813 + 7.474 \times 10^{-4}T$ with T in °C).[26] For **8a**, this gives a molecular volume of $V_M \approx 699$ Å^3 at 130 °C. This allows us to calculate the molecular area A_M as $2V_M/d \approx 42.2$ Å. This value closely corresponds to the area of the square basis of the tetragonal lattice ($a^2 = 40.6$ Å^2). Consequently, the unit cell contains indeed two molecules, in accordance with $Z \approx 2.0$.

Based on the parameters calculated above, a structural model is proposed for the molecular arrangement within the T phases of **3a–12a** (Figure 11). For this model, the following issues were taken into account:

1) The coulombic interactions demand strict alternation of positive and negative charges, and this can only be achieved by placing the cations and anions in the corners and centres of the square basis of the tetragonal lattice. Since there are two molecules (two cations and two anions) per unit cell, the pyrrolidinium and bromide ions are not juxtaposed in single layers, but superposed on top of one another to form double layers. A single-layer molecular arrangement, as represented schematically in Figure 12, is not possible, because of the dimensions of the unit cell of the tetragonal lattice: one side of the square basis of the unit cell measures only 6.37 Å (as deduced above), while the ionic radius of one bromide anion is 1.95 Å and the width of a pyrrolidinium ring is approximately 4.3 Å (as estimated with Chem3D).

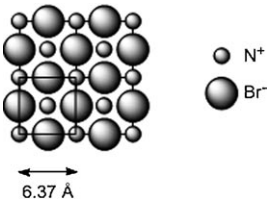

Figure 12. Top view of a theoretically possible single-layer molecular arrangement for the T phase, which satisfies the requirements of charge alternation and the appearance of two molecules per unit cell. However, this arrangement should be discarded for the T phases exhibited by compounds **3a–12a**, because the dimensions of the unit cell are too small.

2) The thickness of an ionic sublayer d_0, estimated to be 9.9 Å, is large enough to accommodate two pyrrolidinium cations on top of one another, with the positively charged nitrogen atoms located in the upper and lower plane of the ionic sublayer, respectively. In this way, the alkyl chains extend above and below the ionic sublayer to create the aliphatic sublayers.
3) The surface area of the square basis ($a^2 = 40.6$ Å^2) indeed corresponds to the area of two long alkyl chains and thus to two molecules per unit cell. (Although they do not contain an elongated rigid core, the molecules are considered to be in an "upright" position. In fact, tilted fluid phases have never been found in amphiphilic liquid crystals without rigid cores).[57]
4) The alkyl chains are in their extended conformation and are interdigitated. For all compounds, the layer thickness d is indeed equal to about 1.37 times the calculated length L of a cation in its most extended conformation (Table 2). The ratio d/L slightly decreases on going from $n = 12$ (1.43) to $n = 20$ (1.33), that is, interdigitation of the longer chains is greater.

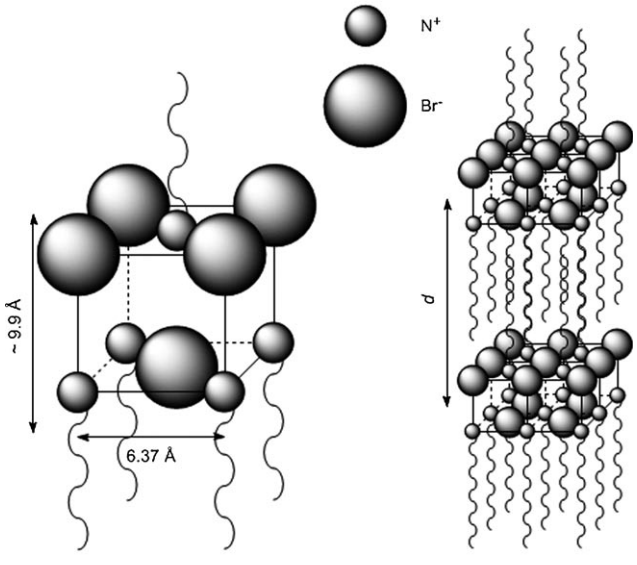

Figure 11. Structural model for the T phases exhibited by **3a–12a**. Left: unit cell of the tetragonal lattice (the carbon and hydrogen atoms of the pyrrolidinium ring and the methyl group on the nitrogen atom of the pyrrolidinium ring are omitted for clarity). Right: two ionic sublayers separated by the aliphatic continuum; d is the layer thickness of the T layers (the length of the alkyl chains is underestimated for clarity).

The molecular packing in the model was also tested with regard to the space-filling requirements by elementary molecular modelling with Chem3D using the cell parameters obtained from X-ray diffraction (Figure 13). The molecular packing found is plausible, as no molecules or ions are suspended in empty space and none overlap.

The proposed model thus strongly resembles the structure of the T phases shown by the *N*,*N*-bis(2-hydroxyethyl)-*N*-methyl-*N*-alkylammonium bromides (without the additional hydrogen bonding of the hydroxyl groups within the ionic sublayers).[4] The calculated density ρ within the ionic sublayers of our pyrrolidinium compounds is 1.37 g cm^{-3}, which is consistent with the value found by Skoulios et al. (1.40 g cm^{-3}) (ρ/mol Å$^{-3} = N_A^{-1}V_0^{-1} = N_A^{-1}Z/a^2d_0$, where N_A is the Avogadro constant; ρ/g cm$^{-3} = 166.06 \times 10^{24}\rho$/mol Å^{-3}, where 166.06 g mol^{-1} is the molecular weight of one ionic

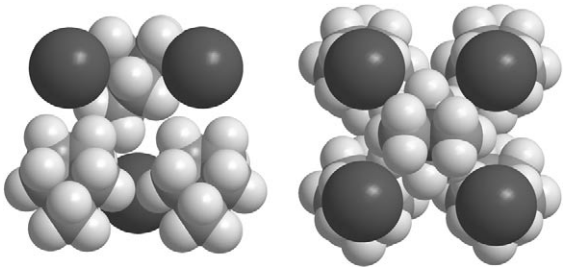

Figure 13. Molecular packing in the T phases exhibited by compounds **3a**–**12a**, as obtained by elementary molecular modelling (Chem3D software). Left: side view of a unit cell of the tetragonal lattice. Right: top view of a unit cell of the tetragonal lattice. For clarity, the long alkyl chains on the cations are replaced by single methyl groups. Before modelling, the structure of a pyrrolidinium cation was energy-minimised by an MM2 calculation within Chem3D. The pyrrolidinium ring is non-planar, with the nitrogen atom sitting above the plane of the four ring carbon atoms.[29]

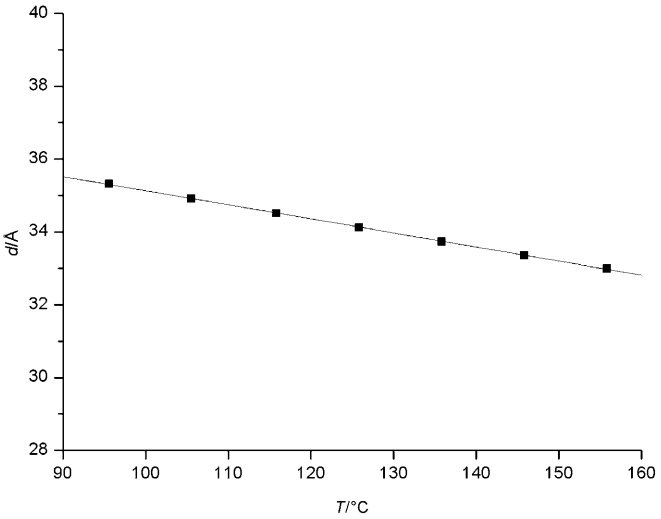

Figure 14. Evolution of the layer thickness d of the SmA phase of **10e** as a function of temperature.

head group).[4] On the contrary, the proposed structure differs from those of all other reported T phases, which contain only one molecule per tetragonal unit cell, although the latter phases were all formed by compounds with two long alkyl chains per cation.[2,5,6] Considering the dimensions of the tetragonal unit cell of our pyrrolidinium compounds, the pyrrolidinium cations are theoretically free to rotate around the axis normal to the smectic layer planes. However, the space-filling model suggests cooperative rotation, whereby rotating cations must share space (as in SmB and crystal B phases).[54]

The T phases of **10c** and **10d** have a smaller layer thickness d in comparison to the T phase of bromide analogue **10a** (Table 2). Furthermore, the molecular area A_M and lattice parameter a are larger (at 130 °C, $A_M = 41.6$ Å^2 for **10a**). This is due to the larger size of the BF_4^- and PF_6^- anions, respectively. The molten alkyl chains are more folded to compensate for the larger molecular area of the ionic head groups in the smectic layers. This explains the smaller d values. In general, however, we propose a similar model for these T phases to that depicted in Figure 11. The BF_4^- and PF_6^- anions can indeed be considered to be negatively charged spheres that resemble a single bromide anion, but with a larger radius. The diffractograms of **10c** and **10d** additionally show the (111), (112), (113), (114) and (115) reflections of a square lattice (Table 2), that is, the smectic layers are correlated (see above). The (210) reflection, however, could not be detected. For **10c** and **10d**, the layer thickness d of the T phase increases slightly with increasing temperature (**10c**: $d = 32.28$ Å at 100 °C, $d = 32.99$ Å at 160 °C; **10d**: $d = 30.33$ Å at 100 °C, $d = 30.95$ Å at 140 °C).

In contrast to the spherical BF_4^- and PF_6^- anions, the linear thiocyanate anion seems to be incompatible with tetragonal ordering; no T phase is observed for **10e**. As expected, the layer thickness d in the SmA phase of **10e** decreases with increasing temperature (Figure 14). The alkyl chains are interdigitated ($L < d < 2L$).

In the case of **10a**, **11a** and **12a** ($n = 18$, 19 and 20, respectively), a SmA phase exists above the T phase at higher temperatures, corresponding to the loss of ordering within the smectic layer planes. This phase, however, only exists over a narrow temperature range. The T–SmA phase transition is accompanied by a decrease in the smectic layer thickness and by an increase of the molecular area (Table 2). The transition can be explained as follows. When the temperature is increased, the volume of the long alkyl chains increases. To counterbalance this increase in volume and molecular area of the alkyl chains, the molecular area of the ionic moieties increases as well (this is necessary for a stable smectic phase). At the T–SmA transition, however, the alkyl chains (and ionic head groups) occupy such a large molecular cross section that the high degree of ordering within the ionic sublayers of the T phase cannot be sustained anymore (as is confirmed by an increase in the thickness of the ionic sublayers, d_0).[4] Nevertheless, for the long-chain compounds **10a**, **11a** and **12a**, the van der Waals interactions between the aliphatic alkyl chains are strong enough to retain the microphase separation between ionic sublayers and aliphatic continuum, which leads to the formation of a disordered SmA phase. For the shorter alkyl chains ($n < 18$), this is not the case (the T phase transforms directly into the isotropic liquid, not via a SmA phase), nor is it the case for **10c** and **10d** ($n = 18$). It may, nevertheless, be expected that for longer alkyl chains ($n > 18$), the corresponding BF_4^- and PF_6^- compounds will show an additional SmA phase, as the van der Waals interactions between the aliphatic alkyl chains will then be sufficiently strong to preserve a microphase separation between ionic sublayers and aliphatic continuum.

Indexing the diffractograms of uranyl complexes **6g**–**12g** was not straightforward (Figure 15). However, for all these salts an orthorhombic lattice could be obtained, with unit cell parameter c equal to the layer thickness d of the meso-

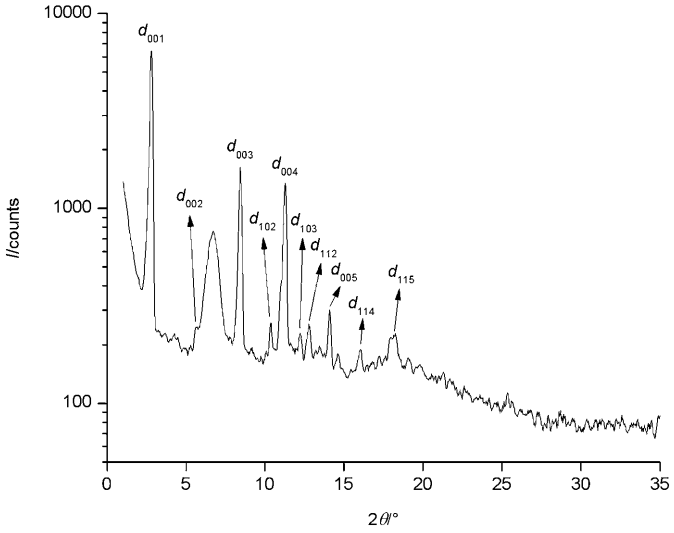

Figure 15. X-ray diffractogram of **6g** in the E phase at 95 °C, represented as the logarithm of the scattering intensity (in counts) versus the scattering angle 2θ (the broad diffraction signal centred at $2\theta \approx 6.5°$ is due to the covering foil used in the experimental set-up).

phase (diffraction data and unit-cell parameters are presented in the Supporting Information). Unfortunately, no reasonable unit-cell parameters *a* and *b* could be found for compound **12g**. The orthorhombic symmetry is consistent only with an orthogonal crystal smectic E phase, which belongs to the class of anisotropic plastic crystal phases.[54,55] This phase has already been observed for *N*-alkylpyridinium salts of $[PdCl_4]^{2-}$ with hexadecyl and octadecyl chains.[48] Interestingly, the corresponding $[PdBr_4]^{2-}$ salts only showed a disordered SmA phase. This was attributed to a lower degree of hydrogen bonding and to size effects. Although no hydrogen bonding can be expected for our $[UO_2Br_4]^{2-}$ complexes, these compounds form a highly ordered E phase. Weak interactions of the protons of the pyrrolidinium cations with the $[UO_2Br_4]^{2-}$ dianions, as observed in the crystal structure of compound **6g** (Figure 1), may be of importance for the formation of the E phase.

Heating the E phase destroys the long-range (intralayer and interlayer) positional order and leads directly to formation of the isotropic liquid in the case of the short-chain compounds (**6g**–**10g**). For the long-chain analogues (**11g** and **12g**), the transition to the isotropic liquid occurs gradually via a SmA phase, by analogy with the T–SmA–I phase sequence observed for the bromide compounds (see above). The diffractogram of the SmA phase of uranyl complexes **11g** and **12g** shows two sharp, equidistant peaks in the small-angle region (corresponding to the lamellar structure), and a diffuse signal in the wide-angle region, centred at about 4.85 Å (corresponding to the lateral short-range order of the molten aliphatic chains). In addition, a diffuse signal centred at about 8.1 Å could be observed (see Supporting Information). This broad reflection is associated with the short-range positional correlation of the $[UO_2Br_4]^{2-}$ dianions within the smectic layers.

Thus, while the cationic head groups and anions of compounds **3a**–**12a** are arranged in a square two-dimensional lattice in the T phase, the ionic fragments of uranyl complexes **6g**–**12g** are ordered in a rectangular two-dimensional lattice. The alkyl chains are interdigitated ($L < d < 2L$). The layer thickness *d* of the E phase increases slightly with increasing temperature (Figure 16). However, it is much more dependent on the number of carbon atoms in the alkyl chain *n*; the layer thickness increases linearly with *n* (Figure 17).

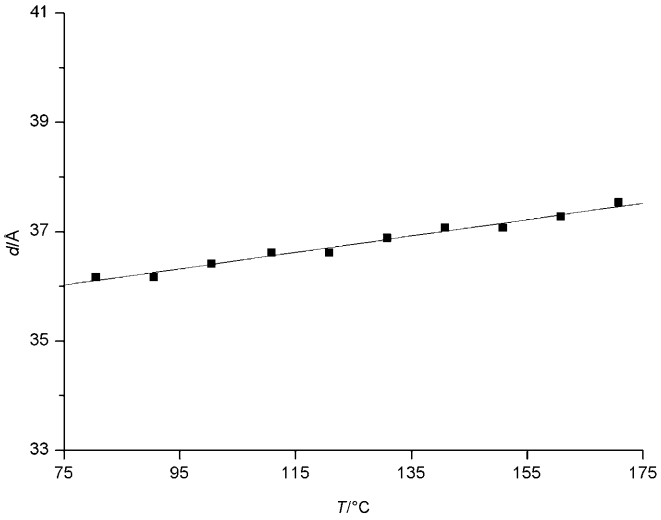

Figure 16. Evolution of the layer thickness *d* of the E phase of **10g** as a function of temperature.

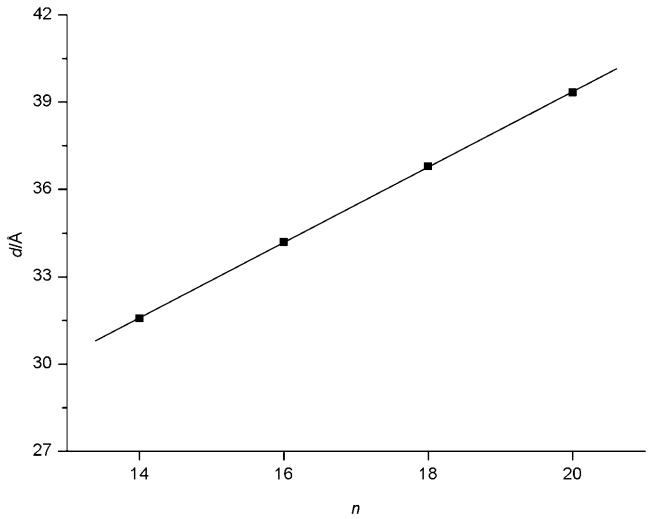

Figure 17. Evolution of the layer thickness *d* of the E phase at 115 °C as a function of the number of carbon atoms *n* in the alkyl chain for the series **6g**–**12g**: $d = 13.5(\pm 0.1) + 1.295(\pm 0.007)n$.

Luminescence properties: Europium(III) complex **10f** exhibits intense red photoluminescence (Figure 18). The luminescence spectrum consists of transitions from the $^5D_0$ excit-

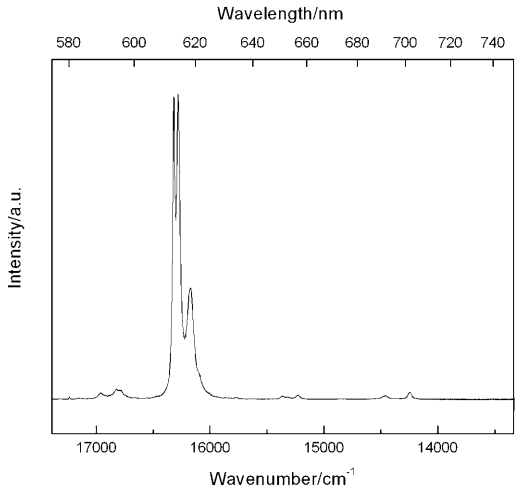

Figure 18. Photoluminescence spectrum of europium(III) complex **10f** in the solid state at room temperature (excitation wavelength: 393 nm).

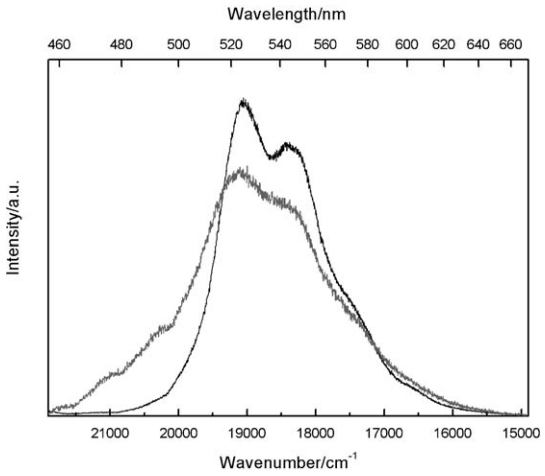

Figure 19. Photoluminescence spectra of uranyl complex **6g** at room temperature (excitation wavelength: 435 nm). Black line: **6g** dissolved in acetonitrile. Grey line: **6g** dissolved in $[C_4mpyrr][NTf_2]$.

ed state to the different J levels of the ^7F ground term (J= 0, 1, 2, 3, 4). The spectrum is dominated by the $^5D_0 \rightarrow {}^7F_2$ line, with emission maximum at 614.3 nm. The intensity ratio $I(^5D_0 \rightarrow {}^7F_2)/I(^5D_0 \rightarrow {}^7F_1)$, obtained by integration of the emission peaks, is 19.9. This value is remarkably high, but is not unusual for europium(III) tetrakis β-diketonate complexes.[58] Thanks to the intense $^5D_0 \rightarrow {}^7F_2$ line, the emitted light has high colour purity. The very weak $^5D_0 \rightarrow {}^7F_0$ line at 580.2 nm (only 3% of the intensity of the magnetic dipole transition $^5D_0 \rightarrow {}^7F_1$) may indicate that the symmetry of the eight-coordinate europium(III) complex is close to an ideal dodecahedron with D_{2d} symmetry (the $^5D_0 \rightarrow {}^7F_0$ line is forbidden in D_{2d} symmetry).

Tetrabromouranyl salts **1g**–**12g** are not luminescent in pure form, probably due to autoquenching.[59,60] However, when these salts were dissolved in acetonitrile or in the ionic liquid *N*-butyl-*N*-methylpyrrolidinium bis(trifluoromethylsulfonyl)imide ($[C_4mpyrr][NTf_2]$), photoluminescence in the visible region of the electromagnetic spectrum could be observed. The luminescence spectra of uranyl complex **6g**, recorded at room temperature, are shown in Figure 19. For both solutions, a broad and intense emission peak was found between 16000 and 21000 cm^{-1}. In contrast to the $[UO_2Cl_4]^{2-}$ species, which shows a distinct vibrational fine structure when dissolved in ionic liquids, no fine structure could be observed for the $[UO_2Br_4]^{2-}$ species, neither in acetonitrile, nor in the ionic liquid.[61–63]

Conclusion

We have synthesised the first series of thermotropic ionic liquid crystals based on the pyrrolidinium cation. The pyrrolidinium compounds show a rich mesomorphism, including highly ordered smectic phases such as the crystal smectic T phase and the crystal smectic E phase, disordered SmA phases and hexagonal columnar phases. Both the alkyl chain length and anion type have great influence on the mesomorphic behaviour. The most interesting feature of (some of) these pyrrolidinium salts is the formation of T phases on heating. The absence of charge delocalisation in the cation seems to be of crucial importance for packing of the ions into a tetragonal lattice. Moreover, large, asymmetric counterions do not seem to be compatible with the highly ordered ionic sublayers of the T phase. To induce disordered phases above the T phase, sufficiently long alkyl chains and small anions are required for the pyrrolidinium compounds. The pyrrolidinium salts containing the $[UO_2Br_4]^{2-}$ fragment are not photoluminescent in the pure, undiluted form, while photoluminescence can be induced by dissolving them in an ionic liquid. In this way, autoquenching is avoided. The europium(III) complex **10f** shows intense red photoluminescence with high colour purity.

Experimental Section

General: Nuclear magnetic resonance (NMR) spectra were recorded on a Bruker Avance 300 spectrometer (operating at 300 MHz for ^1H). Elemental analyses were obtained on a CE Instruments EA-1110 elemental analyser. Electrospray ionisation (ESI) mass spectra were recorded on a Thermo Finnigan LCQ Advantage mass spectrometer. Defect textures of the mesophases were observed with an Olympus BX60 polarising microscope equipped with a LINKAM THMS600 hot stage and a LINKAM TMS93 programmable temperature controller. Microscope glass slides were soaked in concentrated HNO_3 for an hour, washed with distilled water, and finally rinsed with acetone, which was then allowed to evaporate. DSC traces were recorded with a Mettler-Toledo DSC822e module (heating/cooling rate of 10 °C min^{-1}; He atmosphere). Thermal stability was assessed by thermogravimetry in the range from 25 to 400 °C at a heating rate of 10 °C min^{-1} under nitrogen with a TA Instruments SDT Q600 thermal analyser. Powder X-ray diffractograms were recorded with a Bruker AXS D8 Discover diffractometer mounted with a copper X-ray ceramic tube, working at 1.6 kW. The emitted $Cu_{K\alpha}$ radiation (λ= 1.5418 Å) was focussed on the sample by a Göbel mirror. All samples (without a thermal history) were prepared by spreading the powders on a thin cleaned Si wafer. Diffractograms were collected in the Bragg–Bren-

tano reflection geometry ($\theta/2\theta$ set-up) at an angular resolution (in 2θ) of 0.03° per step. The deviation between the temperature on the surface of the sample holder and the set temperature was about 3%. The scattering signal was recorded with a one-dimensional detector (LynxEye detector). Indexation of the powder X-ray diffractograms was performed with the WinX^{POW} program package with the Index & Refine program by using the Werner TREOR algorithm program (allowed error in matching the experimentally observed peaks of $2\theta = 0.05°$).[64,65] Molecular models were obtained with the Chem3D software package from CambridgeSoft. Photoluminescence spectra were recorded on an Edinburgh Instruments FS900 spectrofluorimeter. This instrument is equipped with a xenon arc lamp, a microsecond flashlamp (pulse length: 2 μs) and a red-sensitive photomultiplier (300–850 nm). The excitation wavelength was 393 nm for **10f** and 435 nm for **6g**. The ionic liquid *N*-butyl-*N*-methylpyrrolidinium bis(trifluoromethylsulfonyl)imide was obtained from IoLiTec.

Yellow single crystals of compound **6g** were obtained after three days by slowly evaporating a solution of the compound in ethanol. X-ray intensity data were collected on a SMART 6000 diffractometer equipped with a CCD detector using $Cu_{K\alpha}$ radiation ($\lambda = 1.5418$ Å). The images were interpreted and integrated with the program SAINT from Bruker.[66] **6g**: $C_{38}H_{80}Br_4N_2O_2U$, $M = 1154.70\ g\,mol^{-1}$, monoclinic, $P2_1/n$ (No. 14), $a = 8.5731(3)$, $b = 56.8084(2)$, $c = 10.5237(4)$ Å, $\beta = 113.8850(1)°$, $V = 4686.4(3)$ Å^3, $T = 100(2)$ K, $Z = 4$, $\rho_{calcd} = 1.637\ g\,cm^{-3}$, $\mu(Cu_{K\alpha}) = 13.966\ mm^{-1}$, $F(000) = 2280$, crystal size $0.3 \times 0.2 \times 0.1$ mm, 45996 independent reflections ($R_{int} = 0.0760$). Number of parameters = 428. Absorption correction: multi-scan (SADABS, Bruker 2004). $T_{min} = 0.094$; $T_{max} = 0.247$. Final $R = 0.0486$ for 8254 reflections with $I > 2\sigma(I)$ and $wR_2 = 0.1182$ for all data. The structure was solved by direct methods and refined by full-matrix least-squares techniques on F^2 by using the SHELXTL program package.[67] Non-hydrogen atoms were refined anisotropically and hydrogen atoms in riding mode with isotropic temperature factors fixed at 1.2 *U*(eq) of the parent atoms (1.5 *U*(eq) for methyl groups). CCDC 695524 contains the supplementary crystallographic data for this paper. These data can be obtained free of charge from The Cambridge Crystallographic Data Centre via www.ccdc.cam.ac.uk/data_request/cif.

1a and 2a: The appropriate 1-bromoalkane (1 mol) was added dropwise to an ice-cooled, stirred solution of 1-methylpyrrolidine (1 mol) in dry toluene under an argon atmosphere. The mixture was allowed to warm to room temperature and was stirred for 48 h under an argon atmosphere. The solvent was removed under reduced pressure. The residue was washed carefully with toluene, ethyl acetate and diethyl ether until a white, hygroscopic powder was obtained. The pure compounds were dried in vacuo at 70°C.

1a: Yield: 47%. ^{1}H NMR (300 MHz, CD_3OD, 25°C, TMS): $\delta = 0.91$ (t, $^3J(H,H) = 6.4$ Hz, 3H; CH_3), 1.28–1.50 (m, 10H; CH_2), 1.75–1.90 (m, 2H; NCH_2CH_2), 2.19–2.32 (m, 4H; pyrr. H-3 and H-4), 3.09 (s, 3H; NCH_3), 3.35–3.45 (m, 2H; NCH_2), 3.51–3.66 ppm (m, 4H; pyrr. H-2 and H-5); ^{13}C NMR (75 MHz, CD_3OD, 25°C, TMS): $\delta = 14.54$, 22.68, 23.75, 24.91, 27.64, 30.30, 32.97, 48.90, 65.49, 65.67 ppm; ESIMS (acetonitrile): *m*/*z* (%): 198.4 (100) $[M-Br^-]^+$, 477.2 (10) $[M+M-Br^-]^+$; elemental analysis calcd (%) for $C_{13}H_{28}BrN{\cdot}H_2O$: C 52.70, H 10.21, N 4.73; found: C 52.29, H 10.33, N 4.53.

2a: Yield: 51%. ^{1}H NMR (300 MHz, CD_3OD, 25°C, TMS): $\delta = 0.90$ (t, $^3J(H,H) = 6.4$ Hz, 3H; CH_3), 1.26–1.44 (m, 14H; CH_2), 1.74–1.89 (m, 2H; NCH_2CH_2), 2.19–2.28 (m, 4H; pyrr. H-3 and H-4), 3.08 (s, 3H; NCH_3), 3.34–3.43 (m, 2H; NCH_2), 3.50–3.62 ppm (m, 4H; pyrr. H-2 and H-5); ^{13}C NMR (75 MHz, CD_3OD, 25°C, TMS): $\delta = 14.55$, 22.66, 23.80, 24.90, 27.64, 30.33, 30.48, 30.64, 33.11, 48.94, 65.49, 65.68 ppm; ESIMS (acetonitrile/water (80/20) + 0.1% formic acid): *m*/*z* (%): 226.4 (100) $[M-Br^-]^+$, 533.3 (10) $[M+M-Br^-]^+$; elemental analysis calcd (%) for $C_{15}H_{32}BrN{\cdot}H_2O$: C 55.55, H 10.57, N 4.32; found: C 55.61, H 10.30, N 4.18.

3a: 1-Bromoundecane (1 mol) was added dropwise to an ice-cooled stirred solution of 1-methylpyrrolidine (1 mol) in dry toluene under an argon atmosphere. The mixture was allowed to warm to room temperature and stirred for 12 h under an argon atmosphere. The temperature was increased to 50°C and stirring was continued for 36 h. The pale yellow precipitate was filtered off and washed carefully with toluene, *n*-hexane and ethyl acetate. The residue was vigorously stirred in *n*-hexane for 15 min, filtered off and washed with *n*-hexane and diethyl ether. The pure, white compound was dried in vacuo at 50°C. Yield: 72%. ^{1}H NMR (300 MHz, $CDCl_3$, 25°C, TMS): $\delta = 0.90$ (t, $^3J(H,H) = 6.5$ Hz, 3H; CH_3), 1.19–1.46 (m, 16H; CH_2), 1.71–1.85 (m, 2H; NCH_2CH_2), 2.25–2.38 (m, 4H; pyrr. H-3 and H-4), 3.30 (s, 3H; NCH_3), 3.60–3.69 (m, 2H; NCH_2), 3.77–3.91 ppm (m, 4H; pyrr. H-2 and H-5); ^{13}C NMR (75 MHz, $CDCl_3$, 25°C, TMS): $\delta = 14.02$, 21.59, 22.57, 24.03, 26.33, 29.16, 29.28, 29.37, 29.43, 31.76, 48.61, 64.15, 64.37 ppm; ESIMS (acetonitrile/water (80/20) + 0.1% formic acid): *m*/*z* (%): 240.5 (100) $[M-Br^-]^+$, 559.5 (38) $[M+M-Br^-]^+$; elemental analysis calcd (%) for $C_{16}H_{34}BrN$: C 59.99, H 10.70, N 4.37; found: C 59.68, H 11.07, N 4.34.

4a–12a: The appropriate 1-bromoalkane (1 mol), or for $n > 16$ a solution of the 1-bromoalkane in dry toluene, was added dropwise to a stirred solution of 1-methylpyrrolidine (1 mol) in dry toluene under an argon atmosphere. The mixture was stirred for 48 h at 80°C under an argon atmosphere. A pale yellow precipitate formed and was filtered off and washed carefully with toluene and ethyl acetate. The precipitate was recrystallised from methanol/diethyl ether to obtain a white solid. The pure compounds were dried in vacuo at 50°C.

4a: Yield: 88%. ^{1}H NMR (300 MHz, $CDCl_3$, 25°C, TMS): $\delta = 0.88$ (t, $^3J(H,H) = 6.4$ Hz, 3H; CH_3), 1.26–1.37 (m, 18H; CH_2), 1.74–1.75 (m, 2H; NCH_2CH_2), 2.23–2.39 (m, 4H; pyrr. H-3 and H-4), 3.33 (s, 3H; NCH_3), 3.64–3.69 (m, 2H; NCH_2), 3.85–3.89 ppm (m, 4H; pyrr. H-2 and H-5); ^{13}C NMR (75 MHz, $CDCl_3$, 25°C, TMS): $\delta = 14.51$, 22.06, 23.06, 24.51, 26.81, 29.64, 29.70, 29.76, 29.85, 29.98, 32.29, 49.05, 64.55, 64.82 ppm; ESIMS (acetonitrile/water (80/20) + 0.1% formic acid): *m*/*z* (%): 254.5 (100) $[M-Br^-]^+$, 587.4 (22) $[M+M-Br^-]^+$; elemental analysis calcd (%) for $C_{17}H_{36}BrN$: C 61.06, H 10.85, N 4.19; found: C 60.74, H 11.25, N 4.14.

5a: Yield: 80%. ^{1}H NMR (300 MHz, $CDCl_3$, 25°C, TMS): $\delta = 0.89$ (t, $^3J(H,H) = 6.4$ Hz, 3H; CH_3), 1.19–1.46 (m, 20H; CH_2), 1.71–1.84 (m, 2H; NCH_2CH_2), 2.25–2.38 (m, 4H; pyrr. H-3 and H-4), 3.31 (s, 3H; NCH_3), 3.61–3.69 (m, 2H; NCH_2), 3.77–3.92 ppm (m, 4H; pyrr. H-2 and H-5); ^{13}C NMR (75 MHz, $CDCl_3$, 25°C, TMS): $\delta = 14.13$, 21.68, 22.66, 24.13, 26.44, 29.25, 29.34, 29.40, 29.47, 29.60, 31.89, 48.69, 64.20, 64.46 ppm; ESIMS (acetonitrile/water (80/20) + 0.1% formic acid): *m*/*z* (%): 268.5 (100) $[M-Br^-]^+$, 615.4 (27) $[M+M-Br^-]^+$; elemental analysis calcd (%) for $C_{18}H_{38}BrN$: C 62.05, H 10.99, N 4.02; found: C 61.85, H 11.14, N 3.98.

6a: Yield: 78%. ^{1}H NMR (300 MHz, $CDCl_3$, 25°C, TMS): $\delta = 0.88$ (t, $^3J(H,H) = 6.5$ Hz, 3H; CH_3), 1.26–1.36 (m, 22H; CH_2), 1.69–1.79 (m, 2H; NCH_2CH_2), 2.25–2.37 (m, 4H; pyrr. H-3 and H-4), 3.32 (s, 3H; NCH_3), 3.63–3.69 (m, 2H; NCH_2), 3.81–3.90 ppm (m, 4H; pyrr. H-2 and H-5); ^{13}C NMR (75 MHz, $CDCl_3$, 25°C, TMS): $\delta = 14.13$, 21.69, 22.69, 24.13, 26.44, 29.27, 29.37, 29.48, 29.64, 31.92, 48.70, 64.19, 64.46 ppm; ESIMS (acetonitrile/water (80/20) + 0.1% formic acid): *m*/*z* (%): 282.5 (100) $[M-Br^-]^+$, 643.5 (25) $[M+M-Br^-]^+$; elemental analysis calcd (%) for $C_{19}H_{40}BrN$: C 62.96, H 11.12, N 3.86; found: C 62.76, H 10.71, N 3.83.

7a: Yield: 74%. ^{1}H NMR (300 MHz, CD_2Cl_2, 25°C): $\delta = 0.90$ (t, $^3J(H,H) = 6.3$ Hz, 3H; CH_3), 1.22–1.47 (m, 24H; CH_2), 1.72–1.85 (m, 2H; NCH_2CH_2), 2.24–2.36 (m, 4H; pyrr. H-3 and H-4), 3.26 (s, 3H; NCH_3), 3.56–3.64 (m, 2H; NCH_2), 3.70–3.88 ppm (m, 4H; pyrr. H-2 and H-5); ^{13}C NMR (75 MHz, CD_2Cl_2, 25°C): $\delta = 13.95$, 21.68, 22.75, 24.03, 26.44, 29.24, 29.42, 29.55, 29.71, 31.98, 48.66, 64.30, 64.51 ppm; ESIMS (acetonitrile/water (80/20) + 0.1% formic acid): *m*/*z* (%): 296.6 (100) $[M-Br^-]^+$, 671.6 (46) $[M+M-Br^-]^+$; elemental analysis calcd (%) for $C_{20}H_{42}BrN$: C 63.81, H 11.25, N 3.72; found: C 63.36, H 11.66, N 3.54.

8a: Yield: 76%. ^{1}H NMR (300 MHz, $CDCl_3$, 25°C, TMS): $\delta = 0.88$ (t, $^3J(H,H) = 6.4$ Hz, 3H; CH_3), 1.15–1.48 (m, 26H; CH_2), 1.70–1.87 (m, 2H; NCH_2CH_2), 2.22–2.40 (m, 4H; pyrr. H-3 and H-4), 3.32 (s, 3H; NCH_3), 3.61–3.72 (m, 2H; NCH_2), 3.76–3.96 ppm (m, 4H; pyrr. H-2 and H-5); ^{13}C NMR (75 MHz, $CDCl_3$, 25°C, TMS): $\delta = 14.19$, 21.74, 22.75, 24.20, 26.50, 29.33, 29.43, 29.55, 29.67, 29.74, 31.98, 48.74, 64.23, 64.50 ppm; ESIMS (acetonitrile/water (80/20) + 0.1% formic acid): *m*/*z* (%): 310.6 (100) $[M-Br^-]^+$, 699.6 (30) $[M+M-Br^-]^+$; elemental analysis calcd (%) for $C_{21}H_{44}BrN$: C 64.59, H 11.36, N 3.59; found: C 64.33, H 11.69, N 3.52.

9a: Yield: 80%. ^{1}H NMR (300 MHz, CD_2Cl_2, 25°C): $\delta = 0.91$ (t, $^3J(H,H) = 6.5$ Hz, 3H; CH_3), 1.18–1.51 (m, 28H; CH_2), 1.71–1.85 (m, 2H;

NCH_2CH_2), 2.23–2.37 (m, 4H; pyrr. H-3 and H-4), 3.26 (s, 3H; NCH_3), 3.54–3.64 (m, 2H; NCH_2), 3.70–3.87 ppm (m, 4H; pyrr. H-2 and H-5); ^{13}C NMR (75 MHz, CD_2Cl_2, 25 °C): δ = 14.16, 21.88, 22.96, 24.24, 26.65, 29.45, 29.63, 29.76, 29.97, 32.19, 48.89, 64.57, 64.76 ppm; ESIMS (acetonitrile/water (80/20) + 0.1 % formic acid): *m/z* (%): 324.6 (100) $[M-Br^-]^+$, 727.5 (24) $[M+M-Br^-]^+$; elemental analysis calcd (%) for $C_{22}H_{46}BrN$: C 65.32, H 11.46, N 3.46; found: C 64.91, H 11.73, N 3.33.

10a: Yield: 81 %. ^{1}H NMR (300 MHz, $CDCl_3$, 25 °C, TMS): δ = 0.88 (t, ^3J(H,H) = 6.4 Hz, 3H; CH_3), 1.26–1.36 (m, 30H; CH_2), 1.72–1.75 (m, 2H; NCH_2CH_2), 2.25–2.37 (m, 4H; pyrr. H-3 and H-4), 3.32 (s, 3H; NCH_3), 3.63–3.69 (m, 2H; NCH_2), 3.85–3.88 ppm (m, 4H; pyrr. H-2 and H-5); ^{13}C NMR (75 MHz, $CDCl_3$, 25 °C, TMS): δ = 14.51, 22.06, 23.07, 24.49, 26.81, 29.65, 29.77, 29.89, 30.05, 30.10, 46.05, 64.55, 64.82 ppm; ESIMS (acetonitrile/water (80/20) + 0.1 % formic acid): *m/z* (%): 338.6 (100) $[M-Br^-]^+$, 755.6 (28) $[M+M-Br^-]^+$; elemental analysis calcd (%) for $C_{23}H_{48}BrN$: C 66.00, H 11.56, N 3.35; found: C 65.54, H 11.25, N 3.45.

11a: Yield: 75 %. ^{1}H NMR (300 MHz, CD_2Cl_2, 25 °C): δ = 0.91 (t, ^3J(H,H) = 6.4 Hz, 3H; CH_3), 1.20–1.49 (m, 32H; CH_2), 1.72–1.85 (m, 2H; NCH_2CH_2), 2.24–2.36 (m, 4H; pyrr. H-3 and H-4), 3.26 (s, 3H; NCH_3), 3.55–3.64 (m, 2H; NCH_2), 3.69–3.87 ppm (m, 4H; pyrr. H-2 and H-5); ^{13}C NMR (75 MHz, CD_2Cl_2, 25 °C): δ = 14.15, 21.88, 22.96, 24.24, 26.65, 29.45, 29.63, 29.76, 29.97, 32.19, 48.89, 64.58, 64.76 ppm; ESIMS (acetonitrile/water (80/20) + 0.1 % formic acid): *m/z* (%): 352.6 (100) $[M-Br^-]^+$, 783.5 (12) $[M+M-Br^-]^+$; elemental analysis calcd (%) for $C_{24}H_{50}BrN$: C 66.64, H 11.65, N 3.24; found: C 66.22, H 11.97, N 3.12.

12a: Yield: 76 %. ^{1}H NMR (300 MHz, $CDCl_3$, 25 °C, TMS): δ = 0.88 (t, ^3J(H,H) = 6.5 Hz, 3H; CH_3), 1.25–1.40 (m, 34H; CH_2), 1.69–1.77 (m, 2H; NCH_2CH_2), 2.25–2.37 (m, 4H; pyrr. H-3 and H-4), 3.32 (s, 3H; NCH_3), 3.63–3.68 (m, 2H; NCH_2), 3.82–3.88 ppm (m, 4H; pyrr. H-2 and H-5); ^{13}C NMR (75 MHz, $CDCl_3$, 25 °C, TMS): δ = 14.17, 21.72, 22.73, 24.17, 26.47, 29.31, 29.40, 29.45, 29.55, 29.75, 31.96, 48.70, 64.19, 64.46 ppm; ESIMS (acetonitrile/water (80/20) + 0.1 % formic acid): *m/z* (%): 366.7 (100) $[M-Br^-]^+$, 813.5 (20) $[M+M-Br^-]^+$; elemental analysis calcd (%) for $C_{25}H_{52}BrN$: C 67.24, H 11.74, N 3.14; found: C 67.20, H 11.50, N 3.10.

10b: A solution of **10a** (1.19 mmol) in methanol (6 mL) was heated to 60 °C. An aqueous solution of $LiNTf_2$ (2.38 mmol) was added dropwise and the reaction mixture was stirred for 3 h at 60 °C. Methanol was then removed under reduced pressure. The white precipitate was filtered off, washed with water and dried in vacuo at 50 °C. Yield: 88 %. ^{1}H NMR (300 MHz, $CDCl_3$, 25 °C, TMS): δ = 0.88 (t, ^3J(H,H) = 6.4 Hz, 3H; CH_3), 1.25–1.35 (m, 30H; CH_2), 1.76–1.78 (m, 2H; NCH_2CH_2), 2.23–2.35 (m, 4H; pyrr. H-3 and H-4), 3.08 (s, 3H; NCH_3), 3.30–3.35 (m, 2H; NCH_2), 3.52–3.56 ppm (m, 4H; pyrr. H-2 and H-5); ^{13}C NMR (75 MHz, $CDCl_3$, 25 °C, TMS): δ = 14.25, 21.62, 22.81, 23.99, 26.29, 29.15, 29.23, 29.48, 29.57, 29.73, 29.81, 32.04, 48.54, 64.67, 64.94, 74.11, 113.56, 117.82, 122.06, 126.32 ppm; ESIMS (acetonitrile/water (80/20) + 0.1 % formic acid): *m/z* (%): 338.6 (100) $[M-NTf_2^-]^+$, 956.3 (33) $[M+M-NTf_2^-]^+$, 280.2 (100) $[NTf_2]^-$ (observed in negative mode), 898.1 (68) $[M+NTf_2^-]^-$ (observed in negative mode); elemental analysis calcd (%) for $C_{25}H_{48}F_6N_2O_4S_2$: C 48.53, H 7.82, N 4.53; found: C 48.61, H 8.09, N 4.35.

10c: A solution of **10a** (1.19 mmol) in acetone (10 mL) was heated to 55 °C. $NaBF_4$ (2.38 mmol) was added and the reaction mixture was heated to reflux for 3 h. Inorganic salts were filtered off and washed with acetone. The filtrate was evaporated under reduced pressure to give a white powder. A test with $AgNO_3$ confirmed that no bromide starting compound was present anymore. Residual $NaBF_4$ was removed by dissolving the crude product in dry chloroform, leaving this solution in a refrigerator and filtering the cold solution. The solvent of the filtrate was removed under reduced pressure. This procedure was repeated once. The pure product was dried in vacuo at 50 °C. Yield: 70 %. ^{1}H NMR (300 MHz, $CDCl_3$, 25 °C, TMS): δ = 0.88 (t, ^3J(H,H) = 6.4 Hz, 3H; CH_3), 1.25–1.34 (m, 30H; CH_2), 1.72–1.77 (m, 2H; NCH_2CH_2), 2.23–2.31 (m, 4H; pyrr. H-3 and H-4), 3.10 (s, 3H; NCH_3), 3.33–3.34 (m, 2H; NCH_2), 3.52–3.61 ppm (m, 4H; pyrr. H-2 and H-5); ^{13}C NMR (75 MHz, $CDCl_3$, 25 °C, TMS): δ = 14.53, 22.03, 23.09, 24.31, 26.75, 29.57, 29.77, 29.92, 30.10, 32.32, 48.73, 64.73, 64.78 ppm; ESIMS (acetonitrile/water (80/20) + 0.1 % formic acid): *m/z* (%): 338.6 (100) $[M-BF_4^-]^+$, 763.5 (25) $[M+M-BF_4^-]^+$; elemental analysis calcd (%) for $C_{23}H_{48}BF_4N$: C 64.93, H 11.37, N 3.29; found: C 64.71, H 11.03, N 3.23.

10d: A solution of **10a** (1.19 mmol) in methanol/water (60/40, 10 mL) was heated to 60 °C. An aqueous solution of KPF_6 (2.38 mmol) was added dropwise and the reaction mixture was stirred for 3 h at 60 °C. A white precipitate formed, and was filtered off and washed with water. A test with $AgNO_3$ confirmed that no bromide starting compound was present anymore. The pure product (which completely dissolved in dry chloroform, that is, there was no residual KPF_6) was dried in vacuo at 50 °C. Yield: 98 %. ^{1}H NMR (300 MHz, $CDCl_3$, 25 °C, TMS): δ = 0.88 (t, ^3J(H,H) = 6.5 Hz, 3H; CH_3), 1.25–1.34 (m, 30H; CH_2), 1.73–1.77 (m, 2H; NCH_2CH_2), 2.22–2.32 (m, 4H; pyrr. H-3 and H-4), 3.05 (s, 3H; NCH_3), 3.26–3.32 (m, 2H; NCH_2), 3.51–3.53 ppm (m, 4H; pyrr. H-2 and H-5); ^{13}C NMR (75 MHz, $CDCl_3$, 25 °C, TMS): δ = 14.53, 21.67, 23.09, 24.23, 26.68, 29.51, 29.77, 29.91, 29.92, 30.13, 32.32, 48.77, 64.82, 64.99 ppm; ESIMS (acetonitrile/water (80/20) + 0.1 % formic acid): *m/z* (%): 338.6 (100) $[M-PF_6^-]^+$, 821.4 (35) $[M+M-PF_6^-]^+$, 628.1 (12) $[M+PF_6^-]^-$ (observed in negative mode); elemental analysis calcd (%) for $C_{23}H_{48}F_6NP$: C 57.12, H 10.00, N 2.90; found: C 56.90, H 9.98, N 2.99.

10e: KSCN (36.00 mmol) was added to a solution of **10a** (18.00 mmol) in acetone (150 mL) at 55 °C. The mixture was stirred for 48 h at 55 °C under an argon atmosphere with exclusion of light. The warm reaction mixture was filtered to remove the precipitated KBr. The precipitate was washed with warm acetone and warm chloroform. The solvent of the filtrate was removed under reduced pressure, and the residue was dissolved in dry chloroform. The precipitated residual KBr and the excess of KSCN were filtered off. The solvent of the filtrate was removed under reduced pressure, and the residue was dissolved in dry chloroform again. This solution was left to stand in a freezer overnight. The formed precipitate was filtered off. The solvent of the filtrate was removed under reduced pressure. This procedure was repeated once. The pure, white to pinkish product was dried in vacuo at 50 °C. Yield: 84 %. ^{1}H NMR (300 MHz, $CDCl_3$, 25 °C, TMS): δ = 0.88 (t, ^3J(H,H) = 6.5 Hz, 3H; CH_3), 1.18–1.48 (m, 30H; CH_2), 1.75–1.88 (m, 2H; NCH_2CH_2), 2.31–2.42 (m, 4H; pyrr. H-3 and H-4), 3.25 (s, 3H; NCH_3), 3.49–3.57 (m, 2H; NCH_2), 3.67–3.82 ppm (m, 4H; pyrr. H-2 and H-5); ^{13}C NMR (75 MHz, $CDCl_3$, 25 °C, TMS): δ = 14.26, 22.05, 22.82, 24.28, 26.57, 29.33, 29.50, 29.64, 29.82, 32.05, 48.74, 64.82, 131.48 ppm; ESIMS (acetonitrile/water (80/20) + 0.1 % formic acid): *m/z* (%): 338.7 (100) $[M-SCN^-]^+$, 734.5 (40) $[M+M-SCN^-]^+$; elemental analysis calcd (%) for $C_{24}H_{48}N_2S$: C 72.66, H 12.20, N 7.06; found: C 72.28, H 11.82, N 7.03.

10f: 2-Thenoyltrifluoroacetone (1.46 mmol) was dissolved in ethanol (4 mL), and NaOH (1.46 mmol, 1 mol L^{-1} aqueous solution) was added. The mixture was stirred for 10 min. Then a solution of **10a** (0.37 mmol) in ethanol (5 mL) was added. The mixture was heated to 50 °C. A solution of $EuCl_3 \cdot 6H_2O$ (0.37 mmol) in water (2.5 mL) was added dropwise and the mixture was stirred for 1.5 h at 50 °C with exclusion of light. A yellow precipitate formed and was filtered off and washed with cold water and with cold ethanol. The pure product was dried in vacuo at 50 °C. Yield: 56 %. ESIMS (acetonitrile/water (80/20) + 0.1 % formic acid): *m/z* (%): 338.6 (100) $[M-[Eu(tta)_4]^-]^+$, 1037.1 (100), $[Eu(tta)_4]^-$ (observed in negative mode); elemental analysis calcd (%) for $C_{55}H_{64}EuF_{12}NO_8S_4$: C 48.03, H 4.69, N 1.02; found: C 48.00, H 4.67, N 1.09.

1g–12g: A solution of $UO_2Br_2 \cdot xH_2O$ (1 mol) in ethanol was added dropwise to a stirred solution of the appropriate *N*-alkyl-*N*-methylpyrrolidinium bromide **1a–12a** (2 mol) in ethanol. The reaction mixture was heated to reflux for 2 h. Then the solvent was removed under reduced pressure. The crude product was recrystallised twice from a minimal amount of 1-butanol/ethanol (2/1; **1g–2g**) or from a minimal amount of ethanol (**4g–12g**) to obtain yellow crystals (crystals formed in the refrigerator for the short-chain compounds). The pure compounds were dried in vacuo at 40 or 50 °C.

1g: Yield: 17 %. ESIMS (acetonitrile/water (80/20) + 0.1 % formic acid): *m/z* (%): 198.3 (100) $[M-C_{13}H_{28}N^+-[UO_2Br_4]^{2-}]^+$, 475.2 (17) $[M-[UO_2Br_4]^{2-}+Br^-]^+$; elemental analysis calcd (%) for $C_{26}H_{56}Br_4N_2O_2U$: C 31.66, H 5.72, N 2.84; found: C 31.78, H 5.89, N 2.72.

2g: Yield: 18%. ESIMS (acetonitrile/water (80/20)+0.1% formic acid): *m/z* (%): 226.3 (100) $[M-C_{15}H_{32}N^+-[UO_2Br_4]^{2-}]^+$, 531.2 (18) $[M-[UO_2Br_4]^{2-}+Br^-]^+$; elemental analysis calcd (%) for $C_{30}H_{64}Br_4N_2O_2U$: C 34.56, H 6.19, N 2.69; found: C 34.52, H 6.24, N 2.52.

4g: Yield: 20%. ESIMS (acetonitrile/water (80/20)+0.1% formic acid): *m/z* (%): 254.5 (100) $[M-C_{17}H_{36}N^+-[UO_2Br_4]^{2-}]^+$, 587.3 (12) $[M-[UO_2Br_4]^{2-}+Br^-]^+$; elemental analysis calcd (%) for $C_{34}H_{72}Br_4N_2O_2U$: C 37.17, H 6.61, N 2.55; found: C 37.38, H 6.33, N 2.55.

5g: Yield: 23%. ESIMS (acetonitrile/water (80/20)+0.1% formic acid): *m/z* (%): 268.6 (100) $[M-C_{18}H_{38}N^+-[UO_2Br_4]^{2-}]^+$, 615.5 (20) $[M-[UO_2Br_4]^{2-}+Br^-]^+$; elemental analysis calcd (%) for $C_{36}H_{76}Br_4N_2O_2U$: C 38.38, H 6.80, N 2.49; found: C 38.22, H 6.99, N 2.40.

6g: Yield: 31%. ESIMS (acetonitrile/water (80/20)+0.1% formic acid): *m/z* (%): 282.5 (100) $[M-[C_{19}H_{40}N]^+-[UO_2Br_4]^{2-}]^+$, 645.3 (7) $[M-[UO_2Br_4]^{2-}+Br^-]^+$; elemental analysis calcd (%) for $C_{38}H_{80}Br_4N_2O_2U$: C 39.53, H 6.98, N 2.43; found: C 39.46, H 7.15, N 2.38.

7g: Yield: 34%. ESIMS (acetonitrile/water (80/20)+0.1% formic acid): *m/z* (%): 296.5 (100) $[M-C_{20}H_{42}N^+-[UO_2Br_4]^{2-}]^+$, 671.3 (12) $[M-[UO_2Br_4]^{2-}+Br^-]^+$; elemental analysis calcd (%) for $C_{40}H_{84}Br_4N_2O_2U$: C 40.62, H 7.16, N 2.37; found: C 40.41, H 7.09, N 2.45.

8g: Yield: 40%. ESIMS (acetonitrile/water (80/20)+0.1% formic acid): *m/z* (%): 310.5 (100) $[M-C_{21}H_{44}N^+-[UO_2Br_4]^{2-}]^+$, 699.4 (5) $[M-[UO_2Br_4]^{2-}+Br^-]^+$; elemental analysis calcd (%) for $C_{42}H_{88}Br_4N_2O_2U$: C 41.66, H 7.33, N 2.31; found: C 41.59, H 7.47, N 2.26.

9g: Yield: 38%. ESIMS (acetonitrile/water (80/20)+0.1% formic acid): *m/z* (%): 324.5 (100) $[M-C_{22}H_{46}N^+-[UO_2Br_4]^{2-}]^+$, 727.4 (12) $[M-[UO_2Br_4]^{2-}+Br^-]^+$; elemental analysis calcd (%) for $C_{44}H_{92}Br_4N_2O_2U$: C 42.66, H 7.49, N 2.26; found: C 42.49, H 7.17, N 2.31.

10g: Yield: 43%. ESIMS (acetonitrile/water (80/20)+0.1% formic acid): *m/z* (%): 338.6 (100) $[M-C_{23}H_{48}N^+-[UO_2Br_4]^{2-}]^+$, 757.4 (5) $[M-[UO_2Br_4]^{2-}+Br^-]^+$; elemental analysis calcd (%) for $C_{46}H_{96}Br_4N_2O_2U$: C 43.61, H 7.64, N 2.21; found: C 43.21, H 7.80, N 2.12.

11g: Yield: 45%. ESIMS (acetonitrile/water (80/20)+0.1% formic acid): *m/z* (%): 352.6 (100) $[M-[C_{24}H_{50}N]^+-[UO_2Br_4]^{2-}]^+$, 783.5 (11) $[M-[UO_2Br_4]^{2-}+Br^-]^+$; elemental analysis calcd (%) for $C_{48}H_{100}Br_4N_2O_2U$: C 44.52, H 7.78, N 2.16; found: C 44.47, H 7.60, N 2.23.

12g: Yield: 41%. ESIMS (acetonitrile/water (80/20)+0.1% formic acid): *m/z* (%): 366.6 (100) $[M-C_{25}H_{52}N^+-[UO_2Br_4]^{2-}]^+$, 811.6 (10) $[M-[UO_2Br_4]^{2-}+Br^-]^+$; elemental analysis calcd (%) for $C_{50}H_{104}Br_4N_2O_2U$: C 45.39, H 7.92, N 2.12; found: C 45.22, H 8.10, N 2.07.

Acknowledgements

K.G. is a Research Assistant of the FWO-Flanders (Belgium). T.C. and K.D. are postdoctoral fellows of the FWO-Flanders. Financial support by the K.U.Leuven (projects GOA 08/03 and IDO/05/005) and by the FWO-Flanders (project G.0508.07) is gratefully acknowledged. Part of the uranyl bromide salt was kindly provided by Diederik Huys. C,H,N elemental analyses were performed by Dirk Henot. Mass spectra were measured by Bert Demarsin. Thermogravimetric traces were recorded by Dimitri Soccol. Powder X-ray diffractograms were recorded by Dr. Jan D'Haen and Bart Ruttens (UHasselt, Institute for Materials Research).

[1] K. Binnemans, *Chem. Rev.* **2005**, *105*, 4148–4204.
[2] E. Alami, H. Levy, R. Zana, P. Weber, A. Skoulios, *Liq. Cryst.* **1993**, *13*, 201–212.
[3] F. Tittarelli, P. Masson, A. Skoulios, *Liq. Cryst.* **1997**, *22*, 721–726.
[4] M. Arkas, D. Tsiourvas, C. M. Paleos, A. Skoulios, *Chem. Eur. J.* **1999**, *5*, 3202–3207.
[5] K. Ohta, T. Sugiyama, T. Nogami, *J. Mater. Chem.* **2000**, *10*, 613–616.
[6] A. Nikokavoura, D. Tsiourvas, M. Arkas, Z. Sideratou, C. M. Paleos, *Liq. Cryst.* **2002**, *29*, 1547–1553.
[7] F. Artzner, M. Veber, M. Clerc, A. M. Levelut, *Liq. Cryst.* **1997**, *23*, 27–33.
[8] T. Kato, N. Mizoshita, K. Kishimoto, *Angew. Chem.* **2006**, *118*, 44–74; *Angew. Chem. Int. Ed.* **2006**, *45*, 38–68.
[9] M. Yoshio, T. Mukai, H. Ohno, T. Kato, *J. Am. Chem. Soc.* **2004**, *126*, 994–995.
[10] W. Dobbs, J. M. Suisse, L. Douce, R. Welter, *Angew. Chem.* **2006**, *118*, 4285–4288; *Angew. Chem. Int. Ed.* **2006**, *45*, 4179–4182.
[11] A. Taubert, *Angew. Chem.* **2004**, *116*, 5494–5496; *Angew. Chem. Int. Ed.* **2004**, *43*, 5380–5382.
[12] A. Taubert, Z. Li, *Dalton Trans.* **2007**, 723–727.
[13] C. J. Bowlas, D. W. Bruce, K. R. Seddon, *Chem. Commun.* **1996**, 1625–1626.
[14] A. E. Bradley, C. Hardacre, J. D. Holbrey, S. Johnston, S. E. J. McMath, M. Nieuwenhuyzen, *Chem. Mater.* **2002**, *14*, 629–635.
[15] W. Dobbs, L. Douce, L. Allouche, A. Louati, F. Malbosc, R. Welter, *New J. Chem.* **2006**, *30*, 528–532.
[16] C. M. Gordon, J. D. Holbrey, A. R. Kennedy, K. R. Seddon, *J. Mater. Chem.* **1998**, *8*, 2627–2636.
[17] J. D. Holbrey, K. R. Seddon, *J. Chem. Soc. Dalton Trans.* **1999**, 2133–2139.
[18] I. J. B. Lin, C. S. Vasam, *J. Organomet. Chem.* **2005**, *690*, 3498–3512.
[19] G. A. Knight, B. D. Shaw, *J. Chem. Soc.* **1938**, 682–683.
[20] C. Cruz, B. Heinrich, A. C. Ribeiro, D. W. Bruce, D. Guillon, *Liq. Cryst.* **2000**, *27*, 1625–1631.
[21] L. Cui, V. Sapagovas, G. Lattermann, *Liq. Cryst.* **2002**, *29*, 1121–1132.
[22] F. Neve, O. Francescangeli, A. Crispini, J. Charmant, *Chem. Mater.* **2001**, *13*, 2032–2041.
[23] L. Lu, N. Sharma, G. A. N. Gowda, C. L. Khetrapal, R. G. Weiss, *Liq. Cryst.* **1997**, *22*, 23–28.
[24] D. J. Abdallah, A. Robertson, H. F. Hsu, R. G. Weiss, *J. Am. Chem. Soc.* **2000**, *122*, 3053–3062.
[25] H. Chen, D. C. Kwait, Z. S. Gonen, B. T. Weslowski, D. J. Abdallah, R. G. Weiss, *Chem. Mater.* **2002**, *14*, 4063–4072.
[26] K. Goossens, P. Nockemann, K. Driesen, B. Goderis, C. Görller-Walrand, K. Van Hecke, L. Van Meervelt, E. Pouzet, K. Binnemans, T. Cardinaels, *Chem. Mater.* **2008**, *20*, 157–168.
[27] S. Forsyth, J. Golding, D. R. MacFarlane, M. Forsyth, *Electrochim. Acta* **2001**, *46*, 1753–1757.
[28] K. M. Johansson, J. Adebahr, P. C. Howlett, M. Forsyth, D. R. MacFarlane, *Aust. J. Chem.* **2007**, *60*, 57–63.
[29] D. R. MacFarlane, P. Meakin, J. Sun, N. Amini, M. Forsyth, *J. Phys. Chem. B* **1999**, *103*, 4164–4170.
[30] G. A. Baker, S. Pandey, S. Pandey, S. N. Baker, *Analyst* **2004**, *129*, 890–892.
[31] A. M. Dattelbaum, S. N. Baker, G. A. Baker, *Chem. Commun.* **2005**, 939–941.
[32] N. Menschutkin, *Z. Phys. Chem. (Leipzig)*, **1890**, *6*, 41–57.
[33] J. Golding, N. Hamid, D. R. MacFarlane, M. Forsyth, C. Forsyth, C. Collins, J. Huang, *Chem. Mater.* **2001**, *13*, 558–564.
[34] A. J. Hill, J. Huang, J. Efthimiadis, P. Meakin, M. Forsyth, D. R. MacFarlane, *Solid State Ionics* **2002**, *154*, 119–124.
[35] J. Efthimiadis, S. J. Pas, M. Forsyth, D. R. MacFarlane, *Solid State Ionics* **2002**, *154*, 279–284.
[36] S. Clark, J. M. Elliott, J. R. Chipperfield, P. Styring, E. Sinn, *Inorg. Chem. Commun.* **2002**, *5*, 249–251.
[37] J. M. Elliott, J. R. Chipperfield, S. Clark, E. Sinn, *Inorg. Chem.* **2002**, *41*, 293–299.
[38] J. L. Sessler, W. B. Callaway, S. P. Dudek, R. W. Date, D. W. Bruce, *Inorg. Chem.* **2004**, *43*, 6650–6653.
[39] I. Aiello, M. Ghedini, A. Grisolia, D. Pucci, O. Francescangeli, *Liq. Cryst.* **2005**, *32*, 763–769.
[40] T. Cardinaels, J. Ramaekers, D. Guillon, B. Donnio, K. Binnemans, *J. Am. Chem. Soc.* **2005**, *127*, 17602–17603.
[41] J. Shimizu, T. Nogami, H. Mikawa, *Solid State Commun.* **1985**, *54*, 1009–1011.
[42] P. Dynarowicz, M. Godlewska, W. Witko, *Mol. Cryst. Liq. Cryst., Sect. C: Molec. Mater.* **1997**, 8, 309–317.

[43] A. Babai, A. V. Mudring, *Acta Crystallogr. Sect. E: Struct. Rep. Online* **2005**, *61*, o2913–o2915.
[44] C. B. Aakeröy, K. R. Seddon, *Chem. Soc. Rev.* **1993**, *22*, 397–407.
[45] T. Steiner, *Acta Crystallogr. Sect. B: Struct. Sci.* **1998**, *54*, 456–463.
[46] C. B. Aakeröy, T. A. Evans, K. R. Seddon, I. Palinko, *New J. Chem.* **1999**, *23*, 145–152.
[47] G. R. Desiraju, *Acc. Chem. Res.* **2002**, *35*, 565–573.
[48] F. Neve, A. Crispini, S. Armentano, O. Francescangeli, *Chem. Mater.* **1998**, *10*, 1904–1913.
[49] F. Neve, O. Francescangeli, A. Crispini, *Inorg. Chim. Acta* **2002**, *338*, 51–58.
[50] C. Hardacre, J. D. Holbrey, P. B. McCormac, S. E. J. McMath, M. Nieuwenhuyzen, K. R. Seddon, *J. Mater. Chem.* **2001**, *11*, 346–350.
[51] C. K. Lee, H. H. Peng, I. J. B. Lin, *Chem. Mater.* **2004**, *16*, 530–536.
[52] M. Yoshio, T. Ichikawa, H. Shimura, T. Kagata, A. Hamasaki, T. Mukai, H. Ohno, T. Kato, *Bull. Chem. Soc. Jpn.* **2007**, *80*, 1836–1841.
[53] J. Przedmojski, P. Dynarowicz-Łątka, *Phase Transitions* **1999**, *70*, 133–146.
[54] G. W. Gray, J. W. Goodby, *Smectic Liquid Crystals: Textures and Structures*, Leonard Hill, Glasgow, **1984**.
[55] I. Dierking, *Textures of Liquid Crystals*, Wiley-VCH, Weinheim, **2003**.
[56] B. Donnio, B. Heinrich, H. Allouchi, J. Kain, S. Diele, D. Guillon, D. W. Bruce, *J. Am. Chem. Soc.* **2004**, *126*, 15258–15268.
[57] C. Tschierske, *J. Mater. Chem.* **1998**, *8*, 1485–1508.
[58] K. Lunstroot, K. Driesen, P. Nockemann, C. Görller-Walrand, K. Binnemans, S. Bellayer, J. Le Bideau, A. Vioux, *Chem. Mater.* **2006**, *18*, 5711–5715.
[59] P. Benson, A. Cox, T. J. Kemp, Q. Sultana, *Chem. Phys. Lett.* **1975**, *35*, 195–197.
[60] M. D. Marcantonatos, *Inorg. Chim. Acta* **1978**, *26*, 41–46.
[61] P. Nockemann, K. Servaes, R. Van Deun, K. Van Hecke, L. Van Meervelt, K. Binnemans, C. Görller-Walrand, *Inorg. Chem.* **2007**, *46*, 11335–11344.
[62] R. G. Denning, T. R. Snellgrove, D. R. Woodwark, *Mol. Phys.* **1976**, *32*, 419–442.
[63] C. Görller-Walrand, S. De Jaegere, *J. Chim. Phys.* **1973**, *70*, 360–366.
[64] WinX^{POW} 1.06, STOE & Cie GmbH, Darmstadt (Germany), **1999**.
[65] P. E. Werner, L. Eriksson, M. Westdahl, *J. Appl. Crystallogr.* **1985**, *18*, 367–370.
[66] SAINT, Version 5/6.0, Bruker Analytical X-ray Systems Inc., Madison, Wisconsin, **1997**.
[67] SHELXTL-PC, Version 5.1, Bruker Analytical X-ray Systems Inc., Madison, Wisconsin, **1997**.

Received: July 31, 2008
Published online: November 26, 2008

